Journal of Iberian Geology **42 (2) 2016:** 201-226
http://dx.doi.org/10.5209/rev_JIGE.2016.v42.n2.53232

www.ucm.es/info/estratig/journal.htm
ISSN (print): 1698-6180. ISSN (online): 1886-7995

Journal of Iberian Geology
AN INTERNATIONAL PUBLICATION OF EARTH SCIENCES

On the microstructure, growth pattern and original porosity of belemnite rostra: insights from calcitic Jurassic belemnites

M.I. Benito[1,2]*, M. Reolid[3], C. Viedma[4]

[1]*Departamento de Estratigrafía, Universidad Complutense de Madrid, c/ José Antonio Novais 12, 28040 Madrid, Spain.*
[2]*Instituto de Geociencias IGEO (CSIC-UCM). c/ José Antonio Novais 12, 28040 Madrid, Spain.*
[3]*Departamento de Geología, Universidad de Jaén, Campus Las Lagunillas sn, 23071 Jaén, Spain.*
[4]*Departamento de Cristalografía y Mineralogía, Universidad Complutense de Madrid. c/ José Antonio Novais 12, 28040 Madrid, Spain.*

*e-mail addresses: mibenito@ucm.es (M.I.B., *corresponding author); mreolid@ujaen.es (M.R.); viedma@ucm.es (C.V.)*

Received: 15 June 2016 / Accepted: 28 July 2016 / Available online: 10 August 2016

Abstract

Calcitic belemnite rostra are usually employed to perform paleoenvironmental studies based on geochemical data. However, several questions, such as their original porosity and microstructure, remain open, despite they are essential to make accurate interpretations based on geochemical analyses.

This paper revisits and enlightens some of these questions. Petrographic data demonstrate that calcite crystals of the rostrum solidum of belemnites grow from spherulites that successively develop along the apical line, resulting in a "regular spherulithic prismatic" microstructure. Radially arranged calcite crystals emerge and diverge from the spherulites: towards the apex, crystals grow until a new spherulite is formed; towards the external walls of the rostrum, the crystals become progressively bigger and prismatic. Adjacent crystals slightly vary in their c-axis orientation, resulting in undulose extinction. Concentric growth layering develops at different scales and is superimposed and traversed by a radial pattern, which results in the micro-fibrous texture that is observed in the calcite crystals in the rostra.

Petrographic data demonstrate that single calcite crystals in the rostra have a composite nature, which strongly suggests that the belemnite rostra were originally porous. Single crystals consistently comprise two distinct zones or sectors in optical continuity: 1) the inner zone is fluorescent, has relatively low optical relief under transmitted light (TL) microscopy, a dark-grey color under backscatter electron microscopy (BSEM), a commonly triangular shape, a "patchy" appearance and relatively high Mg and Na contents; 2) the outer sector is non-fluorescent, has relatively high optical relief under TL, a light-grey color under BSEM and low Mg and Na contents. The inner and fluorescent sectors are interpreted to have formed first as a product of biologically controlled mineralization during belemnite skeletal growth and the non-fluorescent outer sectors as overgrowths of the former, filling the intra- and inter-crystalline porosity. This question has important implications for making paleoenvironmental and/or paleoclimatic interpretations based on geochemical analyses of belemnite rostra.

Finally, the petrographic features of composite calcite crystals in the rostra also suggest the non-classical crystallization of belemnite rostra, as previously suggested by other authors.

Keywords: Belemnite rostra, *Sepia*, microstructure, geochemistry, diagenesis, non-classical crystallization

Resumen

Los análisis geoquímicos obtenidos en rostros de los belemnites se utilizan habitualmente para llevar a cabo estudios paleoambientales. Sin embargo, hay cuestiones esenciales, como la porosidad y la microestructura original de los belemnites, que están todavía en discusión y que hay que tener en cuenta si se quieren realizar interpretaciones geoquímicas adecuadas.

Los datos petrográficos obtenidos en este trabajo demuestran que los cristales de calcita del rostrum solidum de los belemnites crecen a partir de esferulitos que sucesivamente se desarrollan a lo largo de la línea apical, dando lugar a una microestructura "esferulítica prismática regular". Los cristales de calcita surgen y divergen radialmente desde los esferulitos: hacia el apex, hasta que se forma un nuevo esferulito y hacia los bordes externos del rostro donde los cristales se van haciendo progresivamente mayores y prismáticos. La ligera variación de la orientación del eje-c de los cristales adyacentes explica la extinción ondulante. Al patrón radial, que da lugar a la textura micro-fibrosa de

los cristales de calcita del rostro, se le superpone un bandeado de crecimiento concéntrico.

Los datos petrográficos también indican que los rostros de los belemnites eran originalmente porosos como lo demuestra la naturaleza compuesta de los cristales de calcita que están formados sistemáticamente por dos zonas distintas que están en continuidad óptica: 1) la zona interna es fluorescente, tiene relieve óptico bajo, en microscopia de luz transmitida (TL), color gris oscuro en microscopia electrónica con electrones retrodispersados (BSEM), morfología triangular y contenidos en Mg y Na relativamente altos; 2) la zona exterior no es fluorescente, tiene relieve óptico alto (TL), color gris claro (BSEM), y contenidos en Mg y Na relativamente bajos. La zona fluorescente interior se formó primero, durante el crecimiento de los belemnites y la zona no fluorescente precipitó como un cemento rellenando la porosidad intra- e intercristalina.

Las características petrográficas de los cristales de calcita también sugieren que la cristalización no clásica del esqueleto de los belemnites, como han sugerido algunos autores previamente.

Palabras clave: Belemnites, *Sepia*, microestructura, geoquímica, diagénesis, cristalización no clásica

1. Introduction

Belemnites are usually employed to perform paleoenvironmental studies based on geochemical data (Spaeth *et al.*, 1971; Veizer, 1974; Veizer and Fritz, 1976; Sælen and Karstang, 1989; Anderson *et al.*, 1994; Sælen *et al.*, 1996; Price and Sellwood, 1994, 1997; Podhala *et al.*, 1998; Veizer *et al.*, 1999; Niebuhr and Joachimski, 2002; Price and Gröcke, 2002; Bailey *et al.*, 2003; Rosales *et al.*, 2004a, 2004b; Wierzbowski, 2004; McArthur *et al.*, 2000, 2004, 2007; Dutton *et al.*, 2007; Prokoph *et al.*, 2008; Nieto *et al.*, 2008; Gómez *et al.*, 2008; Wierzbowski *et al.*, 2009; Price and Rogov, 2009; Nunn *et al*., 2009; Nunn and Price, 2010; Alberti *et al.*, 2011; Wierzbowski and Rogov, 2011; Gómez and Goy, 2011; Li *et al.*, 2012; Armendáriz *et al.*, 2012; Ullmann *et al.*, 2015; Veizer and Prokoph, 2015; and many others). It is generally accepted that the preservation conditions of calcitic belemnite rostra, which are distinguished by their original low-magnesium calcite composition, makes them relatively stable and resistant to diagenetic alteration (Veizer, 1974; Sælen, 1989; Podhala *et al.*, 1998; Rosales *et al.*, 2001, Richter *et al.*, 2011, and references therein). Specifically, many authors have suggested that originally calcitic and non-diagenetically altered belemnite rostra, such as those that are analyzed in this study, display a transparent appearance under transmitted light and a lack of luminescence and, thus, most likely retain their original structure, mineralogy and geochemical composition (e.g., Barskov, 1970; Spaeth *et al.*, 1971, 1973; Veizer, 1974; Sælen, 1989; Podhala *et al.*, 1998; Rosales *et al.*, 2001; Wierzbowski and Joachimski, 2007, 2009; Richter *et al.*, 2011; Benito and Reolid, 2012). However, few detailed analyses of belemnite rostra microstructures are available (Müller-Stoll, 1936; Jeletzky, 1966; Barskov, 1970; Spaeth, 1971; Bandel *et al.*, 1984; Bandel and Spaeth, 1988; Sælen, 1989; O'Neil *et al.*, 2003; Dunca *et al.*, 2006; Dauphin *et al.*, 2007; Wierzbowski and Joachimski, 2009; Cuif *et al.*, 2011; Richter *et al.*, 2011), and several questions regarding belemnite growth and original porosity remain open. For example, no agreement exists regarding whether the present prismatic habits of calcite crystals in belemnite rostra are primary (e.g., Bandel *et al.*, 1984; Sælen, 1989; Richter *et al.*, 2011) or a result of recrystallization (e.g., Jeletzky 1966, p. 108; Barskov, 1970; Spaeth *et al.*, 1971, Cuif *et al.*, 2011, p. 426), whether belemnite rostra were originally porous (Spaeth *et al.*, 1971; Spaeth, 1973, 1975; Veizer, 1974; Richter *et al.*, 2003; Florek *et al.*, 2004), or whether the original porosity was of minor importance (Bandel et al,. 1984; Sælen, 1989). During the last 10 years, several authors have used relatively new techniques to study belemnite rostra, such as synchrotron-based X-ray microfluorescence and diffraction (Florek *et al.*, 2004), electron backscatter diffraction (Richter *et al.*, 2011) or atomic force microscopy (Cuif *et al.*, 2011), which have allowed researchers to make interpretations regarding the original biological matter content of belemnite rostra, the undulosity and radial-fibrous fabric of prismatic calcite crystals, and the original sub-micrometer texture and preservation of radial calcite crystals. However, many of the questions that concern the original microstructure and porosity of belemnite rostra are still unresolved, although they have very important implications when paleoclimate and paleoenvironmental interpretations are made on the basis of belemnite rostra geochemistry.

This work is based on the detailed study of fresh-cut and thin and ultra-thin sections of well-preserved Jurassic belemnite rostra under different petrographic techniques and aims to enlighten some of these controversies by demonstrating the spherulithic nature of belemnite rostra microstructures and that the prismatic calcite crystals in the rostra are composite and were formed through an earlier and biologically controlled phase of calcite and a subsequent phase of calcite that was probably non-biologically controlled, which strongly suggests that the belemnite rostra were porous in origin. Moreover, the biologically controlled portions of the crystals are, in turn, internally composite, which suggests that non-classical crystallization processes were involved in the formation of the rostra's calcite crystals, as previously indicated by Cuif *et al.* (2011).

2. Materials and methods

This study is based on the analysis of well-preserved Oxfordian-Lowermost Kimmeridgian belemnites (*Hibolithes* and few *Belemnopsis*) from the Pozo Cañada section (External Prebetic, Betic Cordillera, southeastern Spain; Fig. 1, Table 1). The Pozo Cañada section (PC) crops out on the northern slope of the Sierra del Chortal located in the south-

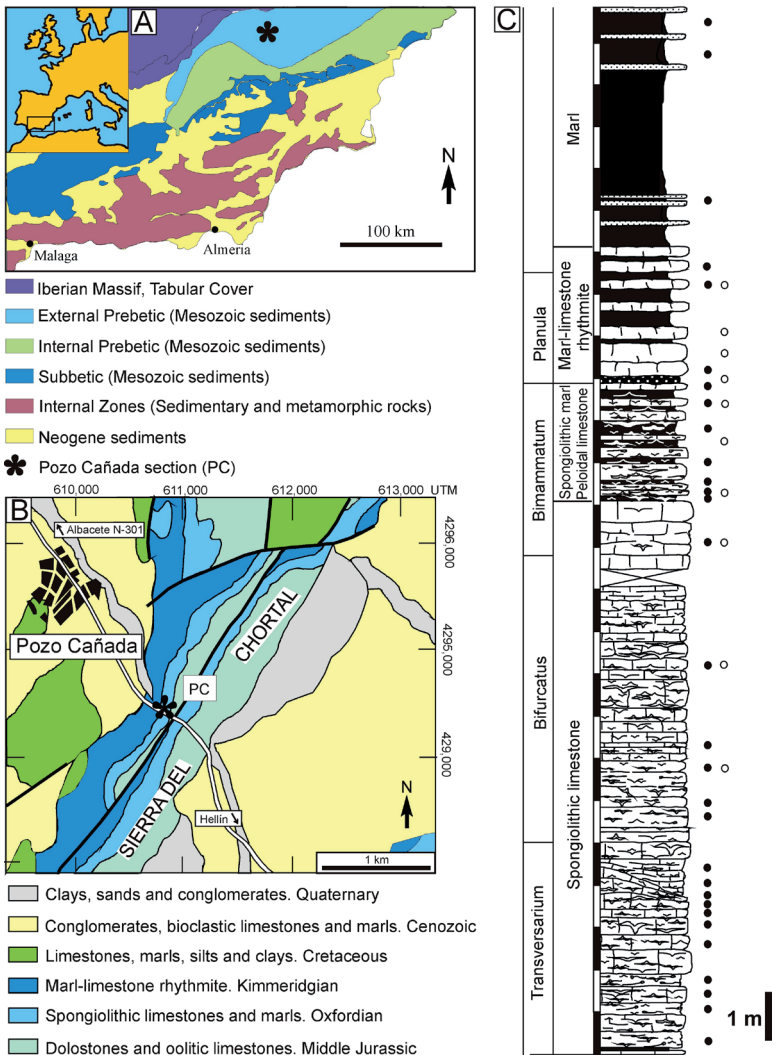

Fig. 1.- A. Geological sketch of southeastern Iberia with location of the studied Pozo Cañada (PC) section (B). C. Pozo Cañada (PC) estratigraphic section with ammonite zones and lithofacies. Black circles correspond to specimens studied by Benito and Reolid (2012) and in this paper. White circles correspond to the new belemnite rostra collected and studied in this paper (see Table 1 for information of each specimen).

east of the village of Pozo Cañada (Albacete province). This section is 20 m thick representing the Middle Oxfordian (Transversarium Zone) to lowermost Kimmeridgian (Planula Zone) composed by spongiolithic limestones, spongiolithic marls-peloidal limestones, marl-limestone rhythmite and marl (Olóriz *et al.*, 2002, 2012). Detailed stratigraphic, petrographical and geochemical analysis of studied belemnites is described in detail in Benito and Reolid (2012).

In addition to samples that were studied by Benito and Reolid (2012), new polished and uncovered thin sections of 10 new belemnites from the same stratigraphic section (Fig. 1, and Table 1 of the Apendix) were prepared to 30 µm thickness for each belemnite rostrum solidum (one longitudinal and one transversal to the growth of the belemnite rostra when possible, Fig. 2). Longitudinal sections of 3 specimens crossed-cut along the apical line; longitudinal sections of the other 7 specimens cross-cut the rostra outwards the apical line (Fig. 2). Thin sections were studied and photographed under conventional microscopy (transmitted, TL, and polarized, PL, light) and cathodoluminescence (CL), entailing the use of a Technosyn cold cathodoluminescent unit MK4 at 20–24 kV with 350–400 mA beam current. All the studied belemnite rostra had a transparent appearance and were non-luminescent, except for the apical line and some growth rings, which had a cloudy appearance and were luminescent (for CL petrographic details see also Benito and Reolid, 2012). Incident-light epifluorescent (FL) microscopy was performed by using a Nikon Y-FL epifluorescence system that was coupled to an Eclipse 6400 POL petrographic microscope. A UV (340–380 nm) excitation filter (400 nm dichroic mirror and 420 nm barrier filter) and a blue light (450–590 nm) excitation filter (505 nm dichroic mirror and 520 nm barrier filter) were used for petrographic work. After examination, thin sections of three specimens were polished again to obtain ultra-thin sections (<15 µm thick). In addition, longitudinal sections of the prong of three specimens of *Sepia orbygnyana* obtained from fisheries were also studied under TL, PL and FL microscopy.

Secondary electron microscopy (SEM) was performed by using a JEOL JSM-820 electron microscope at the Universidad Complutense de Madrid on fresh-cut sections of belemnite rostra. After examination, the samples were etched after immersion in 25% glutardialdehyde for 24 hours. Glutardialdehyde, $CH_2(CH_2CHO)_2$, is an excellent fixing agent of organic matter and is known to react specifically with proteins (Iversen, 1973).

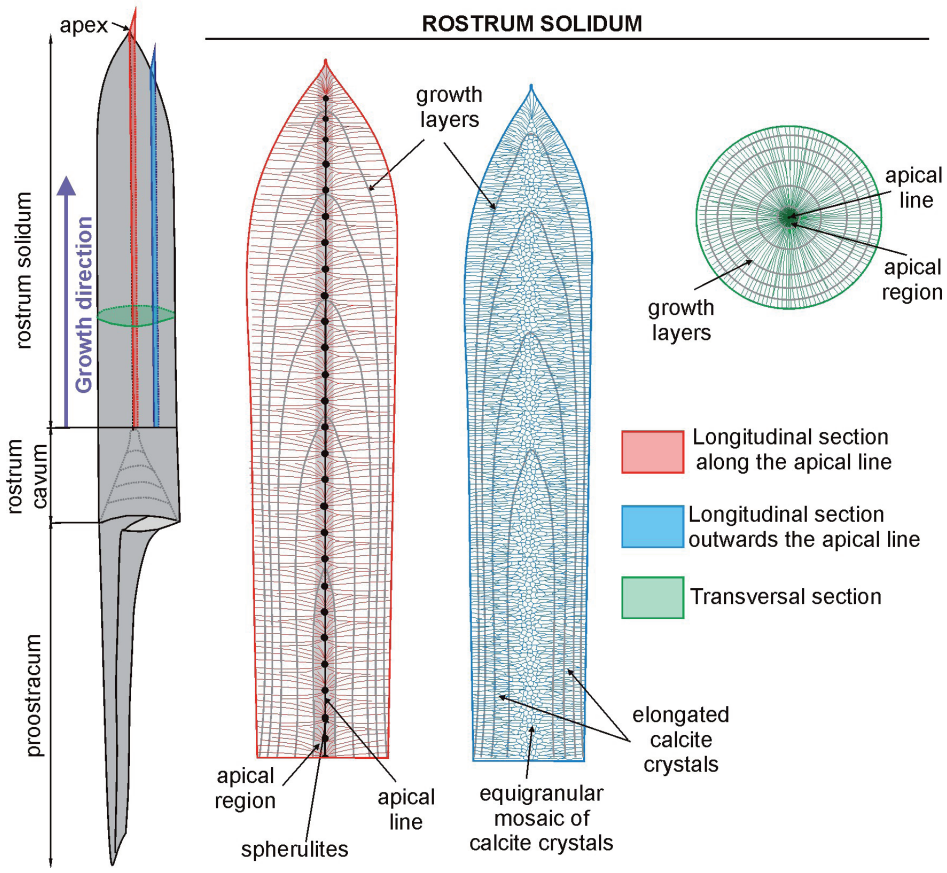

Fig. 2.- Scheme of the anatomy of a belemnite, including the different terms that are used in the text.

Glutardialdehyde easily oxidizes to glutaric acid (Sabatini *et al.*, 1964), and a 25% solution (Merck) that was maintained at a pH of 4.0 has been used to benefit from both the fixing properties of the aldehyde and the etching effect of the acid (Sælen, 1989). After the chemical treatment, the slabs were washed gently with water and ethanol and then dried.

Backscattered scanning electron microscopy (BSEM) and electron microprobe analyses were performed by using a JEOL JXA-8900 electron microprobe that was equipped with five wavelength-dispersive spectrometers at the Universidad Complutense de Madrid. An accelerating voltage of 15 kV, beam current of 10 nA and spot size of 10 µm were used for the spot analyses. The detection limits were 150–180 ppm for Mg, 400–550 ppm for Sr, 140–180 ppm for S, 370–490 ppm for Fe, 450–570 ppm for Mn and 140-180 ppm for Na. For values above the detection limits, the measured precision was better than ± 0.45% for Mg, ± 1.58% for S, ± 3.22 % for Sr, ± 3.2% for Fe, ± 2.8% for Mn, and ± 0.89 % for Na.

The percentage estimation of porosity of belemnites was made by pixel counting methodology proposed by Coimbra and Olóriz (2012) from BSEM images run on Adobe® Photoshop® software CS4.

3. Results

The most characteristic features of the belemnite rostra, which have been described by many authors after observations of both longitudinal and transversal sections (e.g., Müller-Stoll 1936, p. 177; Jeletzky 1966, p. 108; Barskov 1970; Spaeth, 1971, 1975; Spaeth *et al.*, 1971, Bandel *et al.*, 1984; Sælen, 1989; Richter *et al.*, 2011, Benito and Reolid, 2012) include the presence of concentric growth layers or rings; a radial fabric of prismatic calcite crystals that emerge from the apical line and thicken towards the external wall of the rostra; and the crystals' internal micro-fibrous texture, enhanced after etching in 25% glutardialdehyde and in other diluted acids (Sælen, 1989), which more or less perpendicularly traverses the concentric growth pattern.

3.1. SEM observations of fresh-cut sections of belemnite rostra

When the fresh-cut longitudinal and transversal sections of the studied belemnites are analyzed under SEM, it is observed that calcite crystals in the rostrum solidum emerge radially from the apical line towards the apex and external walls of the rostrum (Fig. 2-3A). In the longitudinal sections of very well-preserved rostra, with no observable diagenetic alteration, it is noticeable that calcite crystals emerge radially from successive spherulitic centers of crystal growths that are situated along the apical line (Fig. 3B-F). The nuclei of the spherulites consist of aggregates of isolated and small calcite crystals (around 1 µm in size), which progressively become larger, more elongated and radially arranged in the direction of belemnite growth as hemispherical fans of crystals (Fig.

3B-F). Close to the nuclei of the spherulites, these fans comprise discrete calcite crystals of limited length, commonly no longer than 20-30 μm, which successively grow in between and attached to pre-existing crystals, with their c-axis orientations varying slightly (Fig. 3D-F) and displaying locally curved faces (Fig. 3E). The external surfaces of the crystals are commonly smooth, although in some of them they are rough (Fig. 3F). Towards the apex, the calcite crystals in the spherulites continue growing only until a new spherulite is formed (Fig. 3B-C). However, towards the external walls, the crystals progressively become parallel, longer, and thicker and display prismatic shapes (Fig. 3A-B). The transversal fresh-cut sections show that radially arranged prismatic crystals emerge from the apical line (Fig. 3G-I) and thicken outwards from the apical region (Fig. 3G). Nevertheless, crystals growing among the pre-existing ones are observed outwards from the apical region towards the external wall of the rostra (Fig. 3G). The external surfaces of the crystals may be smooth, but they commonly display micro-fibrous texture (Fig. 3H-I) or slightly rough surfaces (Fig. 3J); moreover, calcite cleavage is commonly observed along broken crystal surfaces (Fig. 3G, J). Concentric growth layers of variable thickness (less than 1 μm, Fig. 3G-J) traverse prismatic crystals and are distinguishable where micro-fibrous fabric is observable (Fig. 3I). Nevertheless, this concentric pattern may have been enhanced and thus is more easily observable after the selective dissolution of some growth layers (Fig. 3H-I) by diagenetic fluids, as previously observed by Benito and Reolid (2012).

After etching in 25% glutardialdehyde, the same pattern of radially arranged crystals is observed in both longitudinal and transversal sections of the rostra; although the prismatic habit become less evident, the micro-fibrous texture is prominent and the concentric growth layering is enhanced (Fig. 4). Locally, the outer portions of some etched crystals display a smooth etching pattern in contrast to the observable fibrous texture in the interiors of the crystals (Fig. 4C); moreover, these crystal boundaries display straight faces and triple junctions (Fig. 4C).

3.2. Observations in thin and ultra-thin sections of the belemnite rostra

3.2.1. Longitudinal sections

Transmitted light, fluorescence and cathodoluminescence

When examining longitudinal thin sections of well-preserved belemnite rostra under transmitted light microscopy (TL), the growth pattern of the belemnites is commonly observable, although the calcite in the apical region typically has cloudy appearance (Fig. 5A) because of diagenetic alteration, which make detailed petrographic observations difficult (see Benito and Reolid, 2012 for a detailed explanation). However, individual spherulites, separated by approximately 100-300 μm (Figs. 3C, 5B-C), are observed along the apical line in ultra-thin longitudinal sections, similarly to what was observed in the fresh-cut sections under SEM. Calcite crystals emerge from spherulites and diverge towards the external walls of the rostra as parallel to sub-parallel prismatic crystals with locally curved faces (Fig. 5B), which display undulose extinction, radial micro-fibrous texture and concentric layering internally (Fig. 5C), the last of which is interpreted as an original growth pattern (Sælen, 1989; Benito and Reolid, 2012). Under FL, concentric growth layering and radial micro-fibrous texture is enhanced (Fig. 5D). Under CL, transparent calcite areas of the rostra are consistently non-luminescent, typical of well-preserved and non-diagenetically altered belemnites; only cloudy areas, such as the apical line and some small fractures are luminescent (Fig. 6A-B). Fluorescent concentric patterns were previously observed by Sælen (1989) and Benito and Reolid (2012), but radial and fluorescent micro-fibrous texture that comprise alternating fluorescent and non-fluorescent microfibers (Fig. 5D), with the latter traversing some of the most intensely fluorescent concentric layers, has not been reported previously.

A similar microstructure has been observed in the longitudinal sections of the prong of *Sepia orbignyana* cuttlebone by Benito *et al*. (2014), who compared the apical spine or prong of some *Sepia* cuttlebone with belemnite rostra, interpreting that the *Sepia* prong is a good analog for belemnite rostrum. In fact, in longitudinal sections of the prong of the cuttlebone, spherulitic prismatic crystals of aragonite are observed as well as concentric growth pattern (Fig. 7) compose of layers formed by radially-arranged aragonite crystals alternating with concentric, organic-rich and not radially-distributed layers, which resemble the structure observed in longitudinal sections of belemnite rostra (see also below).

Once the longitudinal cross-cut section moves away from the apical line (Figs. 2, 3, 5E-F), the spherulitic part of the microstructure is no longer observable, and an equigranular mosaic of sub-euhedral and locally euhedral calcite crystals become recognizable in the middle sector of the rostra, which are the product of transversally cut prismatic calcite crystals (that is, perpendicular to the c-axis). Under FL, concentric layers display overall intense or weak fluorescence (Fig. 5F), which are internally composed of small and fluorescent triangles that are surrounded by non-fluorescent sectors. Moreover, the fluorescent triangles are larger and display more intense FL where the overall fluorescence of the concentric layer is intense compared to the less fluorescent concentric layers, where the fluorescent triangles displays weak FL and are smaller (Fig. 5F).

Under TL, the crystals in the equigranular mosaics, although non-luminescent (Fig. 6C-F), typically display internal zonation with an inner dark zone, which has relatively low optical relief and a commonly triangular shape, and an outer bright zone, in optical continuity, which has a smooth appearance, higher optical relief than the inner zone and commonly sub-euhedral external crystalline boundaries (Fig. 8A-

B). The inner zone of the single crystals sometimes comprises small "patches" (commonly triangular) that are bright and have higher optical relief than the surrounding areas, which are in optical continuity (Fig. 8A-B). The external surfaces of the calcite crystals display triple junctions and comprise boundaries (*sensu* Bathurst, 1975) with common angles of 120º among the three inter-crystalline boundaries, which are also observable within the triangular patches of the inner zones of the crystals (Fig. 8A-B). Small opaque inclusions commonly occur along the boundaries between adjacent crystals and in the triple junctions (Fig. 8A-C).

The fluorescent pattern is coherent with observations under TL: the inner zones of the crystals are fluorescent, while the outer zones are non-fluorescent (Fig. 5C-D), although in some samples, a thin and intensely fluorescent rim is observed along the boundaries between the inner fluorescent and the outer non-fluorescent zones. Moreover, the "patchy" appearance of the inner zones is observable under FL: the low-relief dark parts are fluorescent whilst the triangular dark patches with high optical relief are non-fluorescent or display the same intense fluorescent rim than that observed in the outer zone (Fig. 8C-D). The internal zonation of the calcite crystals is also observable when the longitudinal thin sections cross-cut the belemnite rostra offset from the apical line (Fig. 8E-J): the inner zone is fluorescent, and the outer zone is non-fluorescent. In this case, the shape of the fluorescent inner zone is sometimes triangular but also displays a sub-euhedral shape (Fig. 8I-J).

Progressively towards the external walls of the rostra, the calcite crystals in the mosaic become elongated because they are cut tangentially (Figs. 5E, 8A-G, 9). However, the crystals also display internal zonation under TL and FL: the low-optical-relief inner zones in the crystals are fluorescent, have an elongated triangular shape and sometimes display a "patchy" appearance, and the outer zone of the crystals has an elongated shape and high optical relief and is non-fluorescent (Figs. 8A-D, 9). Towards the external walls of the rostra, the calcite crystals become more elongated and prismatic, displaying a micro-fibrous appearance under TL and/or FL (Fig. 9C-D).

Backscattered electron microscopy (BSEM)

Examination of thin-sectioned rostra under the BSEM reveals a similar pattern to that observed under TL and FL: the fluorescent sectors of the crystals are dark grey in color under BSEM, and the non-fluorescent sectors of the crystals has a light-grey color (compare Figs. 5D and 10A-B; 5F and 10D-E; 8C-D and 10F; 8G and 10G; 9B and 10H-I; 9D and 10K).

When the longitudinal section cross-cut the belemnite rostra along the apical line (Figs 5C-D, 10A-C), a concentric pattern of alternating layers with an overall dark-grey or light-grey color is observed, which is comparable to what was reported under FL, with intensely fluorescent layers being dark grey under BSEM and weakly fluorescent layers being light grey in color. Moreover, a radial micro-fibrous texture is observed under BSEM (Fig. 10B-C), similar to under FL, where non-fluorescent radial sectors traverse fluorescent concentric layers (Fig. 5D). The overall dark-grey concentric layers internally consist of dark-grey sectors, which have an elongated irregular or triangular shape, with the apex of isosceles triangles commonly pointing in the direction of growth (Fig. 10C). Dark-grey sectors are separated by light-grey sectors, which also have a very elongated irregular or triangular shape, with the apex of isosceles triangles commonly pointing in the opposite direction of those in the dark-grey sectors (Fig. 10C). Thus, the dark-grey sectors progressively decrease in width towards the rostral external surface, while the light-grey sectors become progressively predominant until a new dark-grey and fluorescent concentric layer is formed (compare Figs. 5D and 10B-C). Nevertheless, some differences can be observed among the TL, FL and BSEM images because of the different procedures and accuracies of each technique and the effect of the thin section's thickness in TL and FL microscopy, in which the incident light cross through the entire thin sections, in contrast to BSEM.

A similar pattern to what was observed under TL and FL is evident when observing longitudinal sections that do not cross-cut the belemnite rostra along the apical line. The inner zone of the crystals, which had relative low optical relief, a fluorescent nature and a triangular shape, is dark grey

Fig. 3.- Scanning electron microscope (SEM) images of longitudinal (A-F) and transversal (G-J) sections of a freshly cut belemnite rostrum (PC-39). A-C. Successively more detailed images of a rostrum solidum that is cut along the apical line. Calcite crystals begin growing along the apical line and become prismatic towards the external walls of the rostrum (A). Spherulites that are composed of hemispherical fans of calcite crystals are successively distributed along the apical line (B-C). D-E. Detailed images of the nuclei of spherulites. The calcite crystals in the nuclei appear small and isolated in the nuclei and progressively become longer and coalesce into radial structures outwards. The calcite crystals have limited length, and new crystals grow in between pre-existing crystals, with their c-axis orientations varying slightly. Note the curved faces of some crystals (white arrows). F. Detailed image of a spherulite that shows the hemispherical and radial arrangement of crystals. Note the euhedral and rhombohedral crystal terminations, which may display rough surfaces (detailed photograph). G. Transversal section of the rostra that shows the external prismatic shape of the crystals, which thicken outwards from the apical region (to the left). Scattered and poorly preserved concentric pattern traverse prismatic crystals. Concentric pattern is enhanced after dissolution during diagenesis (see Benito and Reolid, 2012 for explanation). Note the cleavage in the broken crystal surfaces (red arrows). Note that outwards the apical region some crystals emerge between preexisting ones (orange arrows) H. Detailed image that shows the micro-fibrous texture of calcite crystals. Relatively thick concentric porous layers formed after dissolution during diagenesis are also observed (pink arrows; see text and Benito and Reolid, 2012 for explanation). I. Detailed image of H that shows thin concentric layers that traverse the micro-fibrous texture (blue arrows). J. Detailed image of prismatic crystals that show relatively smooth surfaces, which display euhedral and small crystalline faces at the crystal surface (yellow arrow). Note the cleavage in the broken crystal surfaces (red arrow).

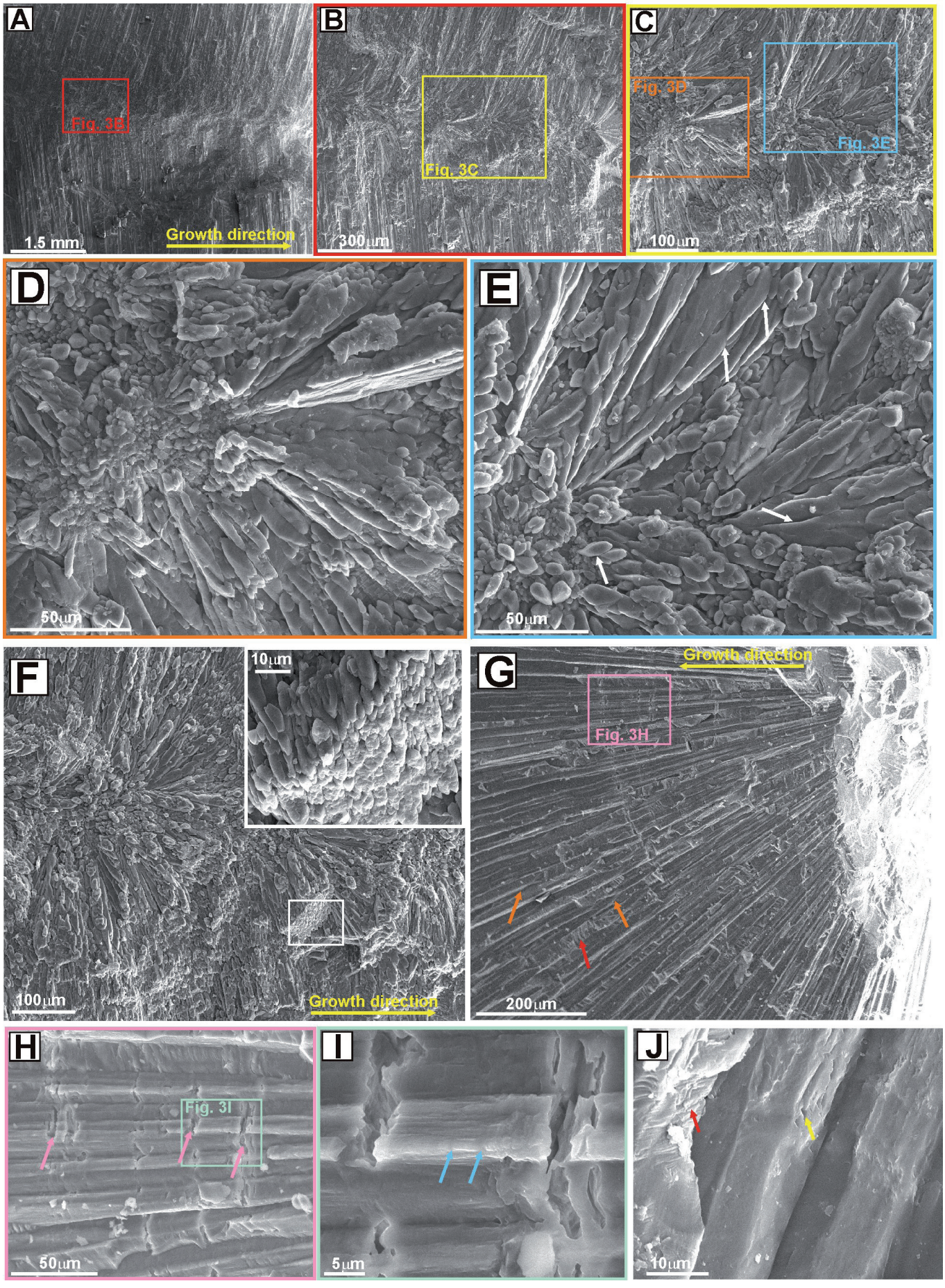
A
Fig. 3B
1.5 mm
Growth direction
B
Fig. 3C
300 µm
C
Fig. 3D
Fig. 3E
100 µm
D
50 µm
E
50 µm
F
10 µm
100 µm
Growth direction
G
Growth direction
Fig. 3H
200 µm
H
Fig. 3I
50 µm
I
5 µm
J
10 µm

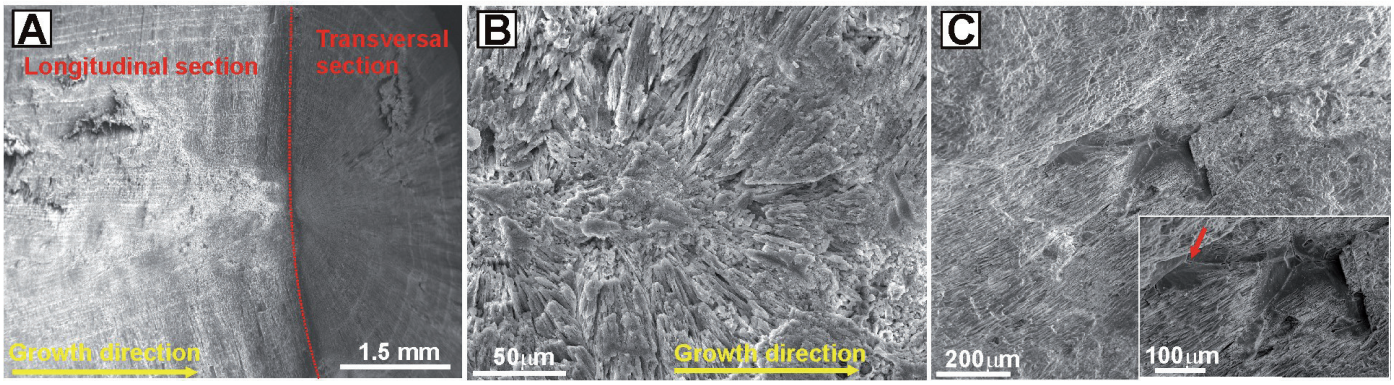

Fig. 4.- A-C. Scanning electron microscopy (SEM) images of the same freshly cut belemnite rostrum as in Fig. 3, after treatment with 25% glutardialdehyde. A. The micro-fibrous texture and the concentric pattern were enhanced compared to the non-etched samples (Fig. 3A and 3G). B. The micro-fibrous texture of the calcite crystals in the spherulite was enhanced after etching (compare to Fig. 3C-E). C. Etched prismatic crystals that show an inner zone with micro-fibrous texture and an outer zone with a homogeneous etching pattern. Note the straight faces and triple junctions (arrow) at the crystal boundaries.

in color under BSEM; the outer zone, which had relatively high optical relief and a non-fluorescent nature, is light grey under BSEM (compare Figs. 5F and 10D-E; 8C-D and 10F; 8G and 10G), although occasionally a thin very light grey rim is observed between both zones (Fig. 10F). Additionally, the "patchy appearance" of the inner zone of the crystals is evident under BSEM, which is comparable to what was observed under TL and FL (Figs. 8C-D and 10F).

Towards the rostral external surface, the crystals, which become elongated as they are cut tangentially (Figs. 8C-D and 10F; 8G and 10G; 9B and 10H-I; 9D and 10K), also display internal zonation under BSEM, which is comparable to what was observed under TL and FL. The fluorescent inner zones of the crystals are dark grey under BSEM, and the non-fluorescent outer zones of the crystals are light grey in color. Moreover, the elongated triangular shape and "patchy" appearance of the inner zones of the crystals, along with triple junctions at the crystal boundaries, were also observable under BSEM (Fig. 10F, G, I). Towards the external walls of the rostra, the dark-grey triangles become more elongated, creating a micro-fibrous appearance, similar to what was observed under FL (compare Figs. 9B and 10H-I; 9D and 10K; 10J).

3.2.2. Transversal sections

Radial and outwardly thickening prismatic crystals that display an internal micro-fibrous texture, undulose extinction and concentric growth layering are observable under TL in transversal thin sections of the well-preserved and non-luminescent rostra (Fig. 6G-H, 11A-B, H). The concentric growth layering is enhanced under FL, displaying alternating weak or intense FL (Fig. 11D), which is often finely zoned inter-

Fig. 5.- Transmitted light (TL, A), polarized light (PL, B, C, E) and fluorescence (FL, D, F) photographs from a slightly oblique longitudinal ultrathin section (see scheme of the cross-cut section in A) of a well-preserved belemnite rostrum (PC 31). The locations of more detailed photographs are shown. A. The belemnite rostrum has a clear and transparent appearance and becomes cloudy in the central area to the right due to diagenetic alteration. Note the concentric growth pattern, which can be observed in the central area. B. Same image as in A under PL. Prismatic calcite crystals emerge from the central area towards the external wall of the rostrum and display undulose extinction. To the right of the image, the section cross-cuts along the apical line and spherulites are observable (see details in C). Prismatic crystals emerge from the spherulites. To the left of the image, the section does not cross-cut the apical line (see scheme in A), and an equigranular mosaic of calcite crystals can be observed in the central area. The crystals become progressively more elongated towards the external walls (see details in E). C. Detailed and counterclockwise rotated image of B that shows the arrangement of crystals where the section cross-cuts the apical line. Successive spherulites (white arrows) are observed along the apical line, from which long prismatic calcite crystals (cutting more or less parallel to their c-axis) emerge and diverge towards the external walls. Concentric growth layering (pink arrows) is poorly observed. D. Similar image as in C under FL (see squares for location). The concentric layers that display alternating intense or weak fluorescence are enhanced compared to those in C (pink arrows). Note that most of the concentric growth layers, which are visible under FL, are not apparent under TL or PL. Also note the radial micro-fibrous texture and non-fluorescent radial sectors that traverse the concentric layers (yellow arrows). The area between the two dotted red line represents the same area as that in Fig. 10B. The area to the right that has the most intense FL corresponds to the diagenetically-altered apical area (see Fig. 6B for CL image of that area). E. Detailed and counterclockwise rotated image of B that shows the arrangement of crystals where the section does not cross-cut the rostrum along the apical line (see scheme in A). Spherulites are not observable, and an equigranular mosaic of calcite crystals is noticeable in the central area, where crystals were cut transversally (perpendicular to their c-axis). The crystals become elongated towards the external walls as they are cut tangentially (to the left and right of the image). The length of these crystals is much smaller than that of the prismatic crystals in C that directly emerge from the spherulites (see B for the transition and the text for an explanation). F. Detailed image of E under FL. A concentric pattern (not noticeable under TL and PL) that displays overall intense or weak fluorescence can be observed. Each sector is composed of small and varyingly fluorescent triangular zones, which are surrounded by non-fluorescent zones. Note that between the fluorescent and non-fluorescent zones, a thin rim of intense FL calcite may be observed. See Fig. 6D for matched image under CL.

nally (Fig. 11E). Non-fluorescent radial sectors traversing the concentric fluorescent pattern are also detected (Fig. 11D-E, I). The concentric growth pattern, although less prominent than in longitudinal sections, appears as layers with an overall dark-grey or light-grey color under BSEM (Fig. 11F-G). In addition, very thin, largely continuous and dark-grey concentric layers of around 1 μm in thickness are observable, which match those that display the most intense fluorescence (compare Fig. 11E and 11G). Equivalent, very-fine concentric layering was observed under SEM in transversal fresh-cut sections (Fig. 3H-I), in which micro-fibrous fabric was observable. Non-fluorescent zones between radial structures were also described by Sælen (1989).

The overall intensely fluorescent and dark-grey concentric layers (Fig. 11E) are internally composed of thick, dark-grey elongated and radial sectors, which have irregular or triangular shapes. The dark-grey sectors are separated by radial and elongated light-grey sectors, which sometimes display symmetrical shapes and commonly have V-shaped terminations (Fig. 11G). The dark-grey and light-grey sectors correspond to fluorescent and non-fluorescent areas, respectively (compare Fig. 11E and 11G). Light-grey sectors are predominant in the overall weakly fluorescent concentric layers and dark-grey sectors are predominant in the overall intense fluorescent concentric layers. In both cases the width of the light- and dark-grey sectors change in the growth direction: the width

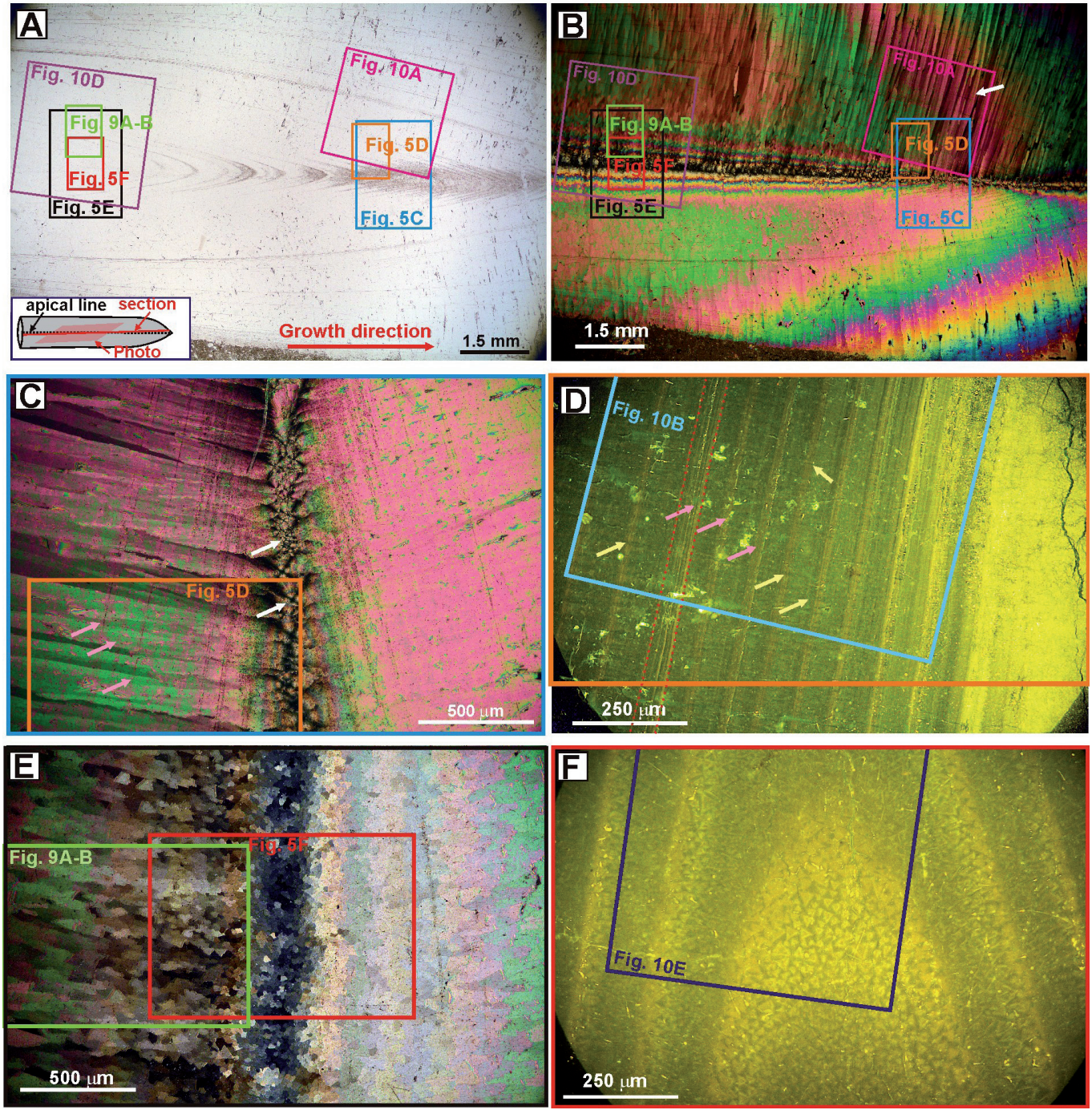

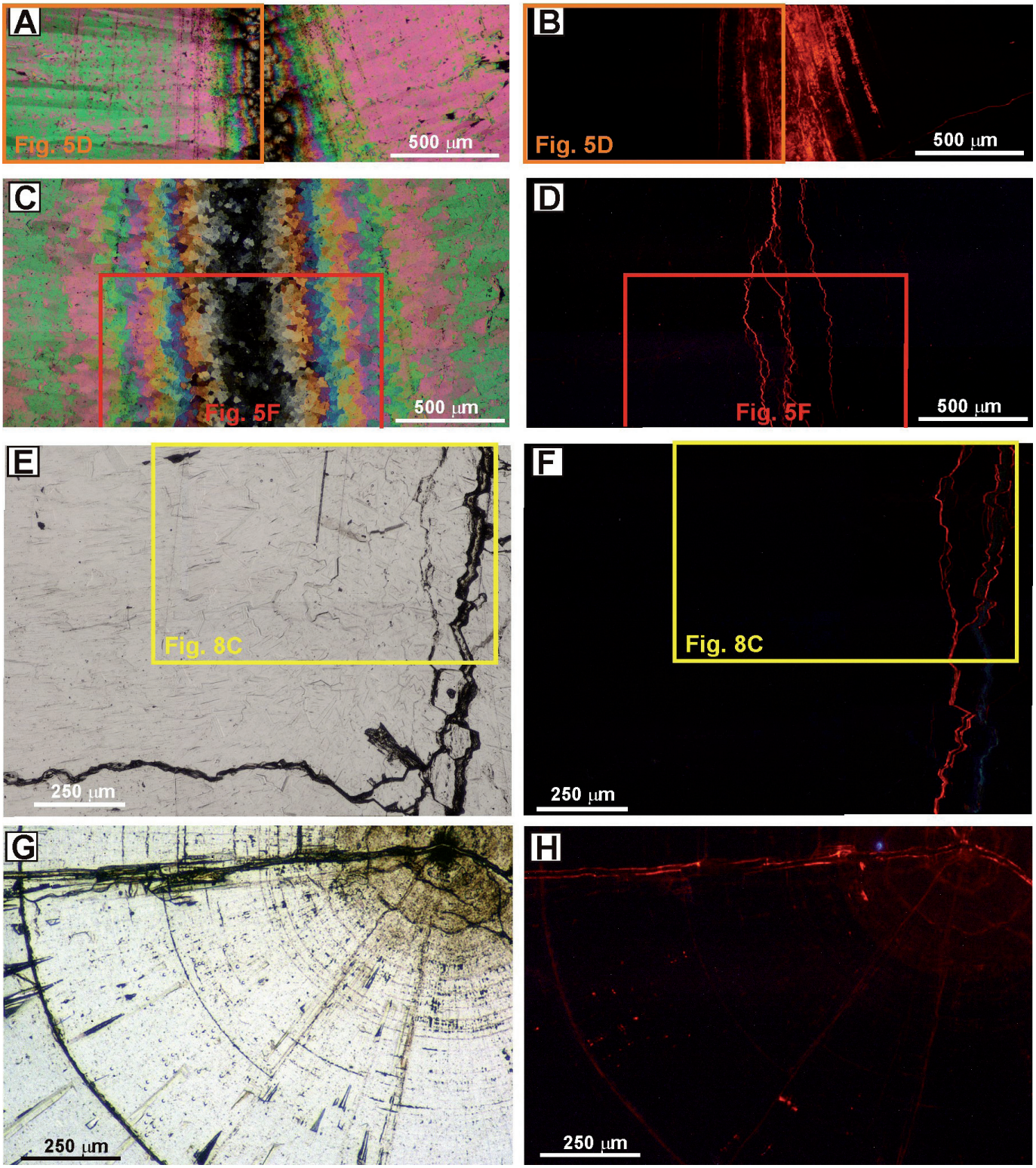

Fig. 6.- Images showing TL and cathodoluminescence (CL) images of belemnite rostra, which match with some of those shown in Figs. 5 and 8. Note that all the rostra are non-luminescent and only the apical area (6B), some small fractures (6D, F, H) and scatter concentric layers (6B, H) are luminescent. A-B. PL and CL images of Fig. 5C-D. C-D. PL and CL images of Fig. 5E-F. E-F. TL and CL images of Fig. 8C-D. G-H. TL and CL images of Fig. 11A, 11D and 11F.

of dark-grey sectors sharply increases just after thin concentric layers are formed and progressively decreases until a new thin concentric layer is formed; the opposite occurs for the light-grey sectors (Fig. 11G). However some differences are observed among the FL images, where the concentric pattern is enhanced, if compared with BSEM images where the radial pattern is enhanced; this is probably a consequence of the effect of the thin section's thickness in FL microscopy,

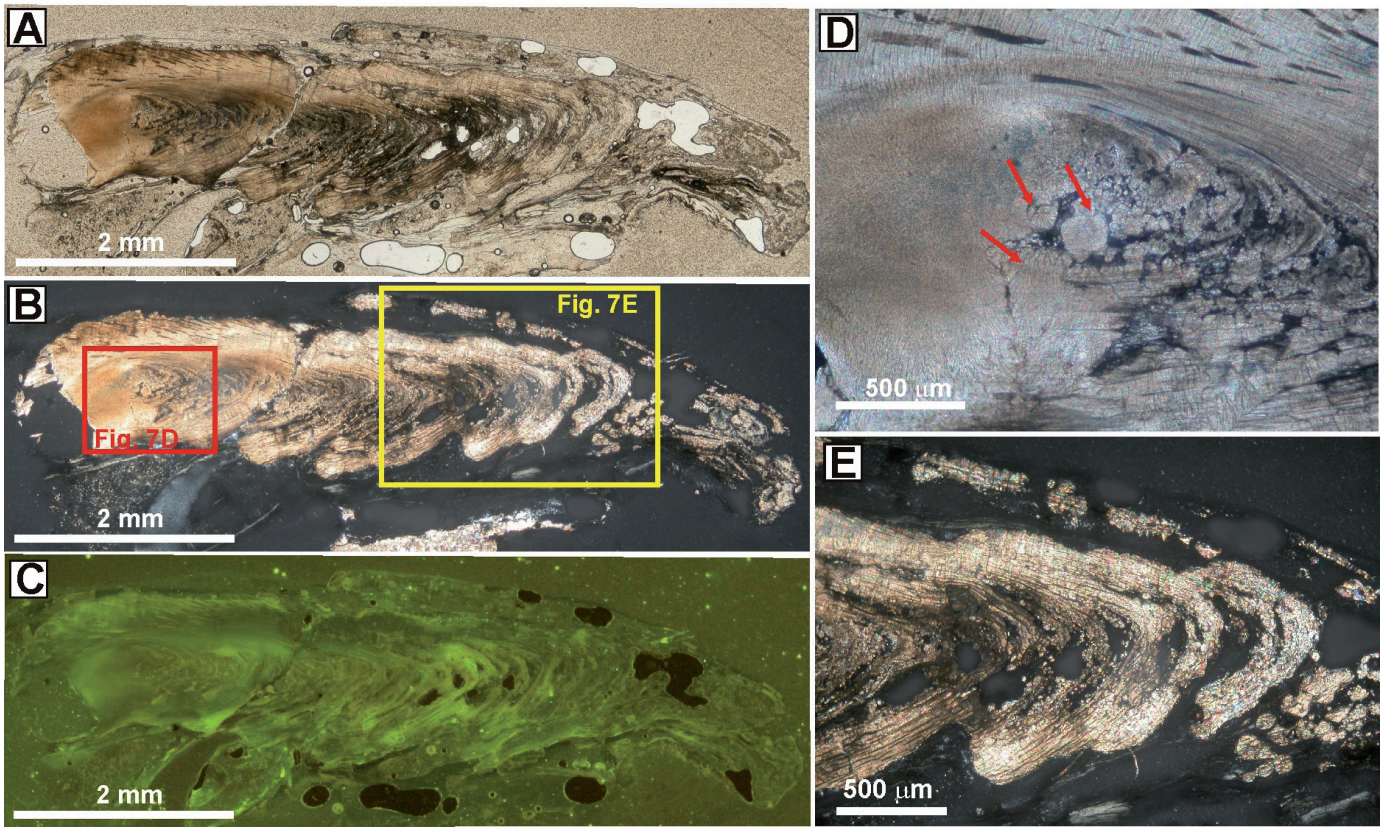

Fig. 7.- Micrographs of longitudinal thin section of the prong of *Sepia orbignyana*, under TL (A), PL (B) and FL (C) microscopy. The red square on B represents the area shown in D and the yellow square on B represents the area shown in E. Note the concentric growth pattern (A-B) of the prong, the spherulites and the radially arranged crystals of aragonite (D: red arrows), and the high intra-skeletal porosity (B-E), which is enhanced in the central area of the prong.

in which the incident light cross through the entire thin section, leading to an apparent increase of the thickness of the fluorescent concentric layers. Neither radial fluorescence nor BSEM zonation were detected or reported by Benito and Reolid (2012), although these features were visible in some of their figures (e.g., their Fig. 4H-L).

Towards the external wall of the rostra, both the fluorescent, dark-grey radial sectors and the non-fluorescent, light-grey radial sectors become more elongated or even fibrous in appearance (Fig. 11H-K).

3.3. Elemental analyses of the belemnite rostra

Microprobe elemental analyses (S, Mg, Sr, Na, Fe and Mn) of the calcite crystals under BSEM (Figs. 12-13) show that dark-grey and fluorescent sectors of calcite crystals have higher Mg and Na contents and similar S content than the light-grey and non-fluorescent sectors (including the light-grey zones of the "patchy" internal zones in the crystals). However, the absolute values are slightly different in each specimen (Figs. 12-13), as previously reported by Benito and Reolid (2012). Sr yields similar values between the dark- and light-grey zones, probably because many of the values are very close or below the detection limit, and thus, the microprobe precision decreases. In addition, both the dark- and light-grey sectors have Fe and Mn contents that are below the detection limits, as expected for non-altered belemnites (e.g., Rosales *et al.*, 2001, Benito and Reolid, 2012) and rarely, some analyses are above the detection limit. This low Fe and Mn contents are coherent with the non-luminescent appearance of the analyzed belemnite rostra and with the elemental (ICP-MS) analyses performed by Benito and Reolid (2012), which recorded Fe and Mn values below 50 and 10 ppm, respectively, in non-luminescent portions of belemnite rostra.

4. Discussion

4.1. Original microstructure and porosity of belemnite rostra

One of the most characteristic and striking features of the microstructure of the rostrum solidum in calcitic belemnites is the fan-like and radial arrangement of prismatic calcite crystals that emerge from the apical line and become thicker towards the external walls of the rostra. Internally prismatic crystals display undulose extinction and micro-fibrous texture (e.g., Bandel *et al.*, 1984, Sælen, 1989; Richter *et al.*, 2011; Benito and Reolid, 2012 and their references therein) and radiaxial-fibrous and subordinate fascicular-optic fibrous fabric (Richter et al., 2011). However, no agreement exists regarding whether the present prismatic habit of crystals is primary (e.g., Bandel *et al.*, 1984; Sælen, 1989; Richter *et al.*, 2011) or a result of recrystallization (e.g., Jeletzky 1966,

p. 108; Barskov, 1970; Spaeth *et al.*, 1971, Cuif *et al.*, 2011, p. 426). Specifically, Spaeth *et al.* (1971) suggested that the primary lattice of belemnite "remained during early processes of diagenesis, but was later successively cemented, especially in those places where the post-mortally decomposed organic matter had disappeared". In addition, Cuif *et al.* (2011) noted that "optical and SEM observation of the rhombohedral fracture of crystalline calcite in the radial prisms of the belemnites provides clear signs of diagenesis" and that "no indications have been reported of organic envelopes surrounding prismatic units that could cause development of a recrystallization process". Additionally, no agreement exists in terms of the original porosity of belemnite rostra: some authors considered that the original porosity was probably of minor importance (Bandel *et al.* 1984; Sælen, 1989), while others suggested that they were originally porous (e.g., Spaeth, 1975; Richter *et al.*, 2003; Florek *et al.*, 2004). In this sense, Spaeth (1975) considered that porosity of belemnite rostrum was about 20% of the rostrum volume, and affirmed that "the fossilized massive calcitic guard of belemnites appears to have been too heavy to support the swimming animal's horizontal living posture". Richter *et al.* (2003) studied Jurassic belemnite rostra under CL and noted that "recent CL-investigations have shown that locally the skeleton (of the belemnite rostra) and the former intraskeletal porosity can be distinguished" and that "further investigations of the reconstruction of the primary porosity would be important because belemnite and brachiopod skeletons are used for the reconstruction of the chemical and isotopic composition of seawater during Earth history". Florek *et al.* (2004) detected an excess of carbon compared to calcium in Jurassic belemnites; with a major decrease in Ca corresponding to the apical line. These authors concluded that "an organic matrix participated in forming the calcium carbonate rostrum". Dunca *et al.* (2006) also observed an excess of carbon in Jurassic belemnite rostra, which they interpreted to possibly reflect the preservation of pristine intra-crystalline and inter-crystalline organic matrix. Meanwhile, Richter *et al.* (2011) examined previous researchers' observations and the complicated luminescent pattern that was observed by Richter *et al.* (2003) in the rostra of some geochemically well-preserved belemnites, questioning "it is at present unclear if the early porosity in belemnite guards and its subsequent occlusion has a significant bearing on the formation of radiaxial calcites?" and noting that "the implication of this may be that belemnite radiaxial calcites represent a composite phase between a biomineral and an early inorganic precipitate with the latter being in optical and crystallographic continuum with its host biomineral". Nevertheless, Richter *et al.* (2011) also indicated that "the presence of biogenic radiaxial calcite, as that of belemnite rostra, in conjunction with the finding of Holocene and Recent radiaxial calcite crystals in meteoric vadose cave environment is considered clear evidence for the primary nature of these fabrics".

Our observations of longitudinal fresh-cut and ultra-thin sections of the rostra showed that the calcite crystals in the

Fig. 8.- A-B. Detailed TL and PL photographs of the longitudinal thin section of a belemnite rostrum (PC 49). An equigranular mosaic of transversally cut calcite crystals is observed to the right of the images. Towards the external wall (to the left), the crystals become elongated as they are cut tangentially. The equigranular mosaic comprises single crystals that display triple junctions (yellow arrows). Opaque inclusions are observed in the triple junctions and along the crystal boundaries (black arrows). Note the internal zonation of single crystals, which display an inner zone with a triangular shape, relatively low optical relief and a commonly patchy appearance (blue arrows) and, in optical continuity, an outer zone with relatively high optical relief and a homogeneous appearance (red arrows). The patches in the inner zone commonly have a triangular shape and relatively higher optical relief than the surrounding sectors. The patches sometimes display triple junctions (green arrows). Progressively towards the external walls, the crystals become elongated and display zonation with an inner sector that displays an elongated triangular shape, relatively low optical relief and a "patchy" to micro-fibrous appearance and, in optical continuity, an external sector with relatively high optical relief. C. TL photograph of the same rostrum and section as in A. The crystal distribution and internal zonation are equivalent to those in A-B (the colors of the arrows are also equivalent). See Fig. 6F for matched CL image. D. Same image as C under fluorescence (FL). The internal zonation of the crystals under FL is similar to what is observed under TL: the low optical relief, triangular and "patchy" inner zone (blue arrows) of single crystals is fluorescent, while the outer zone of crystals with high optical relief and a homogeneous appearance (red arrows) is non-fluorescent. Note that between the fluorescent and non-fluorescent zones, a thin rim of intense FL calcite may be observed. Additionally, the relatively high optical relief patches that are observed in the inner zone of the crystals are non-fluorescent. Towards the external walls (to the left of the photograph) the internal zonation of the elongated crystals is also equivalent to what is observed in C. E-G. Detailed TL, PL and FL images, respectively, of a longitudinal thin section, made outwards the apical line (see Fig. 2), of the belemnite rostrum PC-39. E. Note the transparent appearance and internal zonation of the calcite crystals. In the middle of the photograph, the crystals are cut transversally across their c-axis and display similar zonation to what is observed in A and C. Towards the left and right of the photographs, the crystals become elongated as they are cut tangentially. F. Undulose extinction is observable, although single crystal shapes are poorly observed because of the thickness of the thin section (> 50 μm thick). G. Concentric and fluorescent pattern is observed. The middle of the photograph is composed of small and fluorescent triangular sectors that are surrounded by non-fluorescent sectors, which match those with low optical relief and high optical relief, respectively, under TL. Towards the external walls, the triangular and fluorescent sectors become elongated, exhibiting a micro-fibrous texture. H-J. Detailed TL and FL images of an ultra-thin section (<10 μm thick) of the belemnite rostrum PC-22. H. Note the transparent appearance of the rostrum and the borings that are filled with micrite in both the exterior and interior of the rostrum (pink arrows). I-J. Detailed and clockwise-rotated TL and FL images, respectively, of H that show the internal zonation of the calcite crystals in the rostrum, which display an inner zone with relatively low optical relief, fluorescence and sub-euhedral to triangular shapes (blue arrows) and an outer zone with relatively high optical relief and non-fluorescence (red arrows). Micrite fillings display intense fluorescence. The boring cross-cuts both the fluorescent and non-fluorescent zones of the calcite crystals in the rostrum.

rostrum solidum began growing from spherulithic sectors or spherulites, which successively originated along the apical line during the progressive growth of the belemnite rostra. Spherulites acted as nucleation centers for the calcite crystals, which emerged from the spherulite nuclei as aggregates of isolated and small calcite crystals and progressively became larger and radially arranged, orienting parallel to each other and perpendicular to the external walls (Figs. 3A-F, 5B-C). This arrangement of crystals resembles the "regular spherulithic prismatic" microstructure (*sensu* Carter and Clark, 1985), which was defined as "superficially resembling regular simple prismatic structure, with columnar first order prisms, but with each first order prism consisting of spherulite sector". Bandel *et al.* (1984) reported that "spherulithic sectors" in Jurassic belemnite rostra formed as aggregates of calcite crystals (approximately 1 μm in size) that initially grew

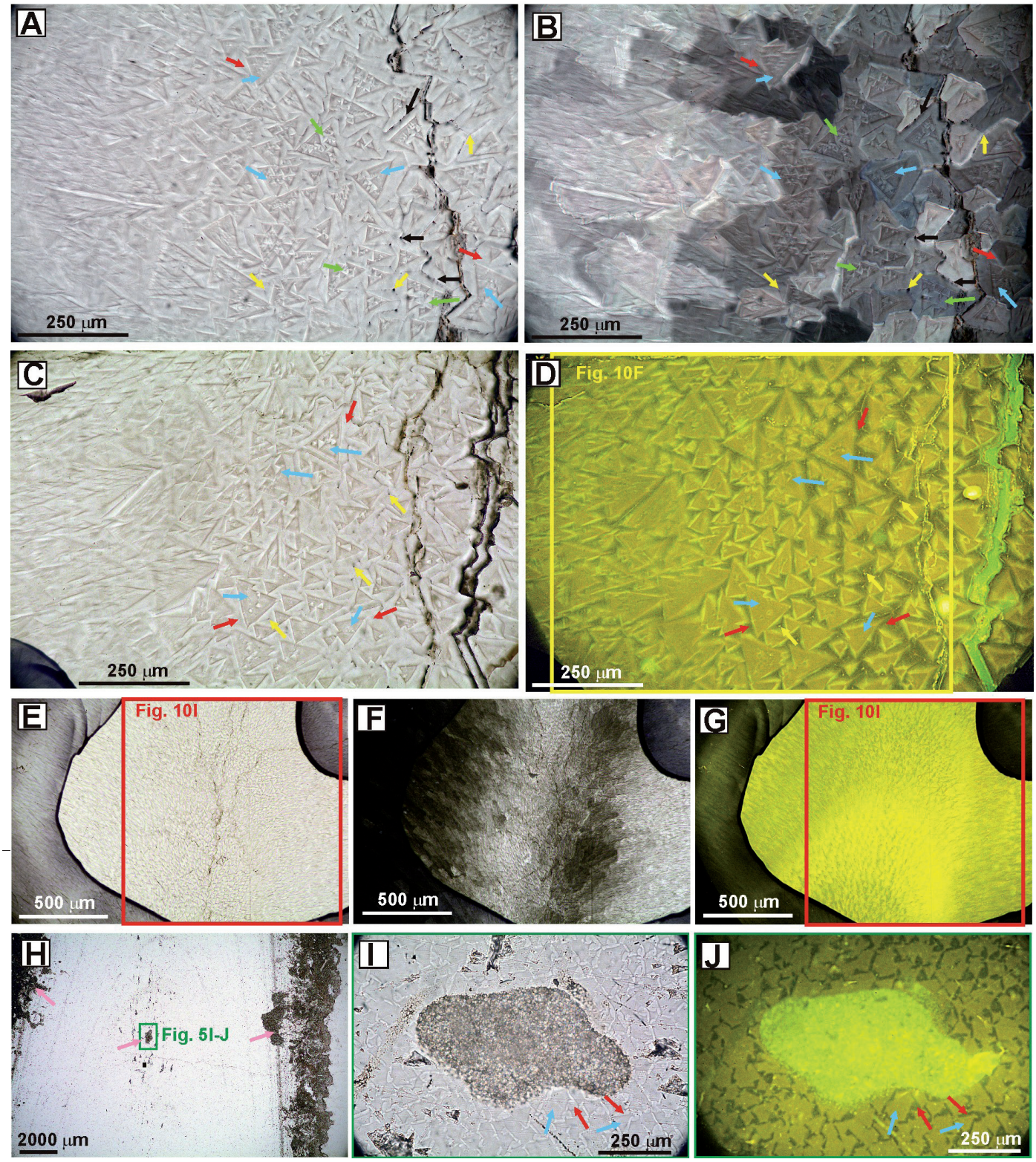

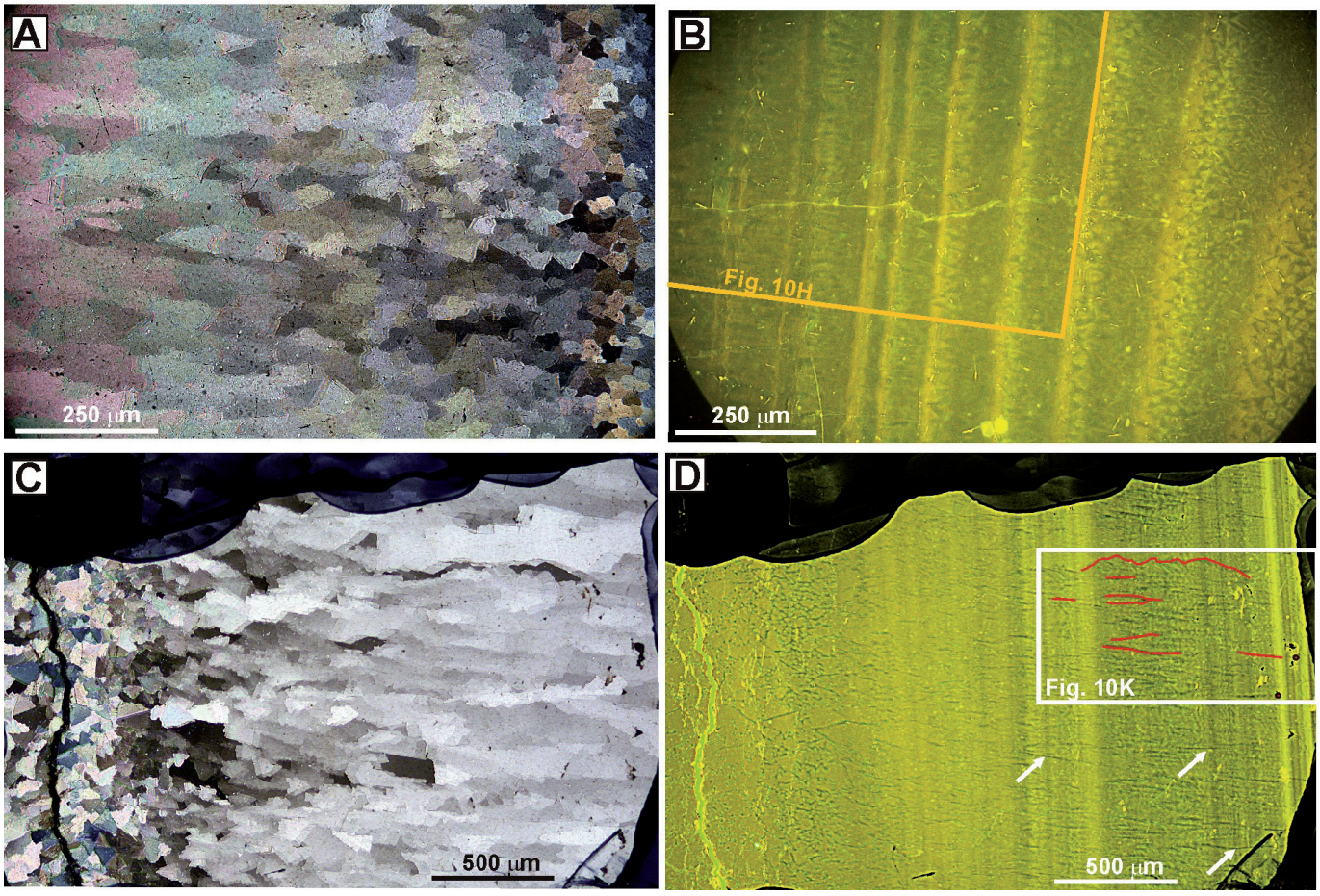

Fig. 9.- A. Detailed PL photograph of the rostrum in Fig. 5E. The crystals become progressively elongated towards the external wall (to the left). B. Same image as in A under FL. This photograph is the leftwards continuation of Fig. 5F. Concentric and fluorescent pattern is observable throughout the rostrum. The crystals that were cut transversally (to the right) are composed of small and fluorescent triangular zones, which are surrounded by non-fluorescent zones, as in Fig. 5F. Towards the external wall, the triangular and fluorescent sectors become progressively more elongated. C. PL photograph of a longitudinal section, made outwards the apical line (see Fig. 2), of a belemnite rostrum (PC 31) that shows the transition from the area where calcite crystals are cut transversally (to the left) to the external wall, where the calcite crystals become elongated and prismatic as they are cut tangentially (to the right). D. Same image as in C that shows concentric FL pattern (not noticeable under PL). To the left, the fluorescent zones or sectors are triangular or sub-euhedral in shape and are surrounded by thin non-fluorescent zones. Towards the external wall (to the right), the triangular and fluorescent zones become progressively more elongated, exhibiting a micro-fibrous texture. The non-fluorescent sectors are long and thin and commonly cross-cut the concentric fluorescent layers (white arrows). The red lines were drawn over some of the non-fluorescent sectors to be compared with those in Fig. 10K.

outwards from the apical line in all directions. However, to our knowledge, this research reports by the first time "regular spherulithic prismatic" microstructure for belemnite rostra. In addition, the calcite crystals become longer and radially arranged outwards from the spherulite nuclei but exhibit limited length because they successively grow in between and attached to pre-existing crystals, with their c-axis orientation varying slightly (Fig. 3D-F). This slight and progressive variation in the orientation of the calcite crystals' c-axis could have led to the undulose extinction that has been observed under polarized light microscopy in the belemnite rostra thin sections by several authors (e.g. Sælen, 1989). This interpretation partially agrees with the conclusion by Richter *et al.* (2011) for biogenic and abiogenic radiaxial-fibrous and fascicular optic-fibrous calcite. These authors proposed to explore the significance of crystal lattice strain and deformation from subtle gradients in Mg/Ca ratios and the kinetic factors during crystal nucleation that might lead to the subsequent generation of crystallites, each with a c-axis that is displaced by a small angle crystal boundary relative to the previous one, as observed in this work (Fig. 10E).

The observations that were made under TL, FL and BSEM show that the calcite crystals are internally composed of fluorescent and dark-grey sectors (or zones) and non-fluorescent and light-grey sectors (Figs. 5, 8-11). These sectors or zones display different shapes depending on whether the section is longitudinal, whether the section cross-cut the belemnite rostra along the apical line, or whether the section is transversal (Fig. 2). The fluorescent and dark-grey calcite has relatively high Mg and Na contents and similar S contents (although the mean S values are slightly higher) compared to the non-fluorescent and light calcite (Figs. 12, 13). In this sense, the fluorescence in biogenic calcite can be activated by organic compounds (e.g., Boto and Isdale, 1985; Cercone *et*

al., 1985; Pedone *et al.*, 1990), and Mg, Na and S are commonly incorporated into biogenic marine calcite (e.g., Busenberg and Plummer, 1985; Pingitore *et al.*, 1995; Cuif *et al.*, 2011). Moreover, the preservation of pristine organic matter is not unusual in well-preserved fossil material (Clark, 1999), especially within crystallites (the intra-crystalline organic matrix of Clark, 2005). In fact, several authors have suggested the presence of original organic matrix in belemnites (Muller-Stoll., 1936; Jeletsky, 1966; Barskov, 1970; Spaeth *et al.*, 1971; Westbroek *et al.*, 1979; Sælen, 1989; Florek *et al.*, 2004; Dunca *et al.*, 2006; Arkhipkin *et al.*, 2012; Wierzbowski and Joachimski, 2009; Wierzbowski, 2013).

Thus, the fluorescent and dark-grey calcite is interpreted to have formed during belemnite rostrum growth from a biologically controlled mineralization process (*sensu* Lowenstam and Weiner, 1989 and Mann, 2001), during which the calcite incorporated organic compounds that cause fluorescence and Mg and Na, each of which exhibit less atomic weight than Ca, resulting in the dark-grey color of the calcite under BSEM. On the other hand, the non-fluorescent and light-grey sectors, although in optical continuity with the fluorescent and dark-grey calcite, would not have incorporated a sufficient amount of organic compounds to activate fluorescence and would have incorporate minor amounts of Mg and Na, which suggests that precipitation occurred at a different time and under different circumstances than the fluorescent calcite. This interpretation is also coherent with observations after etching with glutardialdehyde (Fig. 4C): the etched pattern of the inner zone of some crystals was fibrous in contrast to that in the outer zone, which was smooth, reinforcing the hypothesis of two different stages of calcite precipitation.

Moreover, our observations of longitudinal thin sections, in which calcite prisms were cross-cut transversally or tangentially (Figs 8, 9, 10D-K), strongly suggest that biologically controlled and fluorescent calcite formed prior to the optically continuous and non-fluorescent sectors of the calcite crystals, which would have precipitated during a second stage. In this regard, the petrographic features of the non-fluorescent and light-grey calcite (Figs. 8A-D, 9F) strongly suggest that it precipitated as overgrowths of fluorescent calcite, probably filling inter-crystalline and intra-crystalline pore spaces, thus questioning the origin of the non-fluorescent and light-grey calcite as a product of biologically controlled mineralization. The petrographic features that also support this interpretation include: 1) the sharp, euhedral, and commonly triangular shape of the boundary between the fluorescent and dark-grey inner zone of the crystals and the non-fluorescent and light-grey outer zone and the boundary between the non-fluorescent and light-grey patches, which are included in the fluorescent and dark-grey inner zones (Figs. 8, 10E-I); 2) the internal and triangular-shaped zoning of the outer zone in the crystals as observed under BSEM and FL (Figs. 8D, 10F); 3) the occurrence of plane interfaces in the inter-crystalline boundaries and the abundance of comprise boundaries and triple junctions (see Bathurst, 1975), many of them at 120º (Figs. 4C, 8A-D, 10F, I); 4) the presence of small opaque inclusions along the crystals' boundaries and in the triple junctions (Fig. 8A-C); 5) the absence of fabrics that are characteristic of neomorphic calcite ("all transformations between one mineral and itself or polymorph"; Folk, 1965), such as irregular crystal sizes, wavy or curved inter-crystalline boundaries, and floating relics in the interior of the crystals.

Petrographic observations also revealed that the belemnite rostra did not grow continuously but instead grew periodically, creating the observed concentric growth pattern, as previously reported by Sælen (1989). Moreover, the concentric layers in the longitudinal sections that cross-cut the rostra along the apical line and in the transversal sections (Figs. 5C-D, 9A-C, 11), where calcite prisms are cross-cut more or less parallel to their c-axis, are not homogeneous or continuous; in contrast, the layers are internally composed of radial and elongated sectors that are irregular or triangular in shape and sometimes display dark-grey or light-grey color under BSEM. These dark-grey and fluorescent sectors are interpreted to have formed periodically during belemnite growth as biologically controlled discrete crystalline sectors, leading to the overall intense fluorescence in the concentric growth layers. However, these growth layers were probably originally porous because light-grey and non-fluorescent calcite, which is interpreted to be pore space infillings, traverse the concentric layers and are in between the dark-grey and fluorescent sectors, which are interpreted to have formed under biologically controlled mineralization (Figs. 5D, 10C, 11E-G).

In accordance with this interpretation, Richter *et al.* (2003) showed the diagonal section of the rostrum of a Middle Jurassic belemnite in their Fig. 4d and reported that "skeleton elements" or the "inner parts of the triangles" had intrinsic (non-luminescent) CL, while "cement generations" or the "outer part of the triangles" displayed "Mn-activated (orange)" intrinsic CL, interpreting that the latter precipitated in intra-skeletal porosity. In this sense, Sælen (1989) and Benito and Reolid (2012) observed thin, radial and luminescent areas at the boundaries between calcite crystals in the diagenetically altered belemnites (their Fig. 3D), interpreting that diagenetic alteration was favored by these boundaries. These luminescent areas that were observed by Richter *et al.* (2003) and Benito and Reolid (2012) in diagenetically altered belemnites could be equivalent to the non-fluorescent and light-grey sectors of the studied belemnites but precipitated under different diagenetic conditions (i.e., sub-oxic or reduced conditions) than the studied belemnites, which are well preserved and non-luminescent (Fig. 6) and contain little Fe and Mn (Figs. 12).

All these findings enlighten the controversy of whether belemnite rostra were originally porous, whether the calcite crystals are composite and whether their present prismatic habit is primary. Our observations strongly support that the belemnite rostra were originally porous and that the present prismatic habit of the crystals is secondary and mostly the result of calcite overgrowing within inter- and intra-crystalline

porosity, which was left after biologically controlled belemnite skeletal formation. The porosity, which has been estimated based on the analysis of BSEM images of some rostra (e.g. Fig. 10G), would yield values between 20 and 60%: the lower porosity values were obtained where dark-grey calcite is more abundant and the higher values where light-grey calcite predominates. This porosity values are coherent with those observed in longitudinal sections of the prong of *Sepi*a cuttlebones (Fig.7).

The original porosity was probably larger in the apical region and would have progressively decreased towards the external wall of the rostra, as also occurs in the prong of *Sepia* cuttlebone (Fig. 7). In this sense, the apical line has been considered to be semipermeable, allowing solutions to percolate (e.g., Sturz-Köwing 1960; Stevens and Clayton, 1971), and consists of spherulites, which had been connected to organic fibers (Bandel *et al.*, 1984) or as sectors of the rostra with a higher excess of carbon (porosity increased) with probable remnants of original biological matter (Florek *et al.*, 2004). In fact, the apical line commonly has a cloudy appearance and is luminescent, even in well-preserved belemnites, because of diagenetic alteration (e.g., Spaeth, 1975, Sælen, 1989, Bandel, 1984, Floreck *et al.*, 2004; Dunca *et al.*, 2006, Benito and Reolid, 2012), which suggests that diagenetic fluids easily percolate through this sector because of its relatively higher original porosity, favoring the breakdown of any inter-crystalline organic matter that was present in the rostra. Moreover, our observations suggest that the original porosity was both inter-crystalline and intra-crystalline, as demonstrated by the presence of optically continuous non-fluorescent overgrowths within the biologically controlled fluorescent inner zones of the calcite crystals (Figs. 8A-D, 10F).

4.2. Non-classical growth of a belemnite skeleton?

Another question to address is why the fluorescent and biologically controlled inner zones of the calcite crystals has triangular shapes but are internally formed by smaller triangularly shaped non-fluorescent sectors that are in optical continuity (Figs. 8A-D, 10F). This observation suggests the possibility that small, biologically controlled and iso-orientated calcite crystals were fused into larger crystals, leaving intra- and inter-crystalline pore spaces that were later filled with non-fluorescent calcite. This process is comparable to the non-classical crystallization process, a mechanism that has been proposed in recent years for the biomineralization of several organisms, such as some corals, foraminifers, echinoderms and mollusks (e.g., Cölfen and Antonietti, 2008; Meldrum and Cölfen, 2008; Marin *et al.*, 2011; Cuif *et al.*, 2011; De Yoreo *et al.*, 2015; and references therein). Accord-

Fig. 10.- Backscattered electron microscopy (BSEM) images of longitudinal sections of belemnite rostra. A. BSEM image of the belemnite rostrum in Fig. 5B-D, where the section cross-cuts the apical line (see those figures for the location). Note the concentric layering. B. Detailed image of A that shows the apical region of the rostrum (to the right of the image), which is largely porous, and the concentric layering to the left. Concentric layers display alternating dark-grey or light-grey color. The dark-grey layers correspond to those that display intense FL (the area within the dotted red lines corresponds to that in Fig. 5D), and the light-grey layers correspond to those that display weak FL. The overall dark-grey concentric layers internally consist of dark-grey elongated sectors that are separated by light-grey sectors, which were non-fluorescent in Fig. 5D, and traverse the dark-grey concentric layering. C. Detailed image of A that shows the external area of the rostrum. The concentric dark- to light-grey layering is similar to that in B. As in B, the dark-grey sectors are elongated and irregular or triangular in shape, with the apex of the isosceles triangles commonly pointing in the direction of growth. The width of the dark sectors progressively decreases until a new dark-grey layer is formed. The dark-grey sectors are alternating with radial and elongated light-grey sectors, which may be irregular or triangular in shape (pointing in the opposite direction than the dark-grey ones) and traverse dark-grey concentric layers (yellow arrows). The triangles sometimes have symmetrical shapes (yellow square) and V-shaped terminations (green arrow). D. BSEM image of the same belemnite rostrum where the section does not cut along the apical line (see Fig. 5B, E-F and 9A-B for location). Note the dark- to light-grey concentric layering, which matches that in Figs. 5F and 9B. E. Detailed image of D that shows the area where the calcite crystals are cut transversally across their c-axis. The dark-grey concentric layers correspond to those that had overall intense FL and are composed of dark-grey triangles (fluorescent in Fig. 5F) that are surrounded by light-grey sectors (non-fluorescent in Fig. 5F). Light-grey sectors are more abundant in the concentric layers of the thin section, which display an overall light-grey color and weak FL in Fig. 5F. F. Same image as in Fig. 8C-D under BSEM (arrows; see Fig. 8C-D). The relatively low optical relief and fluorescent zones have a dark-grey color under BSEM, while the non-fluorescent zones with relatively high optical relief display a light-grey color under BSEM. The dark-grey sectors (blue arrows) have a triangular shape and are surrounded by light-grey sectors (red arrows) that may be zoned. The dark-grey triangles internally have a "patchy" appearance because they contain small light-grey sectors, which display triangular or elongated shapes, similar to those that are observed under TL and FL (Fig. 8C-D). The yellow arrows point to the triple junctions that were observed in Fig. 8C. G. Same image as in Fig. 8G under BSEM. Note the alternating zones predominantly composed of dark-grey and light grey elements, respectively, which match those that display intense or weak fluorescence in Fig. 8G. The dark-grey concentric layers are composed of dark-grey triangles, which are surrounded by small light-grey sectors. The dark-grey triangles become smaller in concentric areas that primarily display an overall light-grey color. Note the "patchy" appearance of some of the dark-grey triangles (blue arrows). H. Detailed images of D that show the areas of the rostrum where calcite crystals are cut tangentially (see Fig. 9A-B for location). Concentric dark- to light-grey layering is also observed. The dark-grey concentric layers, which match those that display intense FL (Fig. 9B), consist of dark-grey elongated triangular sectors that are surrounded by light-grey sectors, which become progressively predominant in concentric layers that display weak FL. I. Detailed image of H. Note the "patchy" appearance of some of the dark-grey triangles (blue arrows) and the triple junctions that developed along the crystal boundaries of the light-grey sectors (yellow arrow). J. Detailed image of D that shows the external area of the rostrum. Similar pattern as in H and I can be observed, although the dark-grey triangles are more elongated than those in H and I. K. Same image as in Fig. 9D under BSEM. The dark-grey sectors, which are fluorescent, have an elongated triangular shape and are surrounded by light-grey elongated sectors, which are non-fluorescent in Fig. 9D (for comparison, the red lines and red circles are in the same positions as in Fig. 9D).

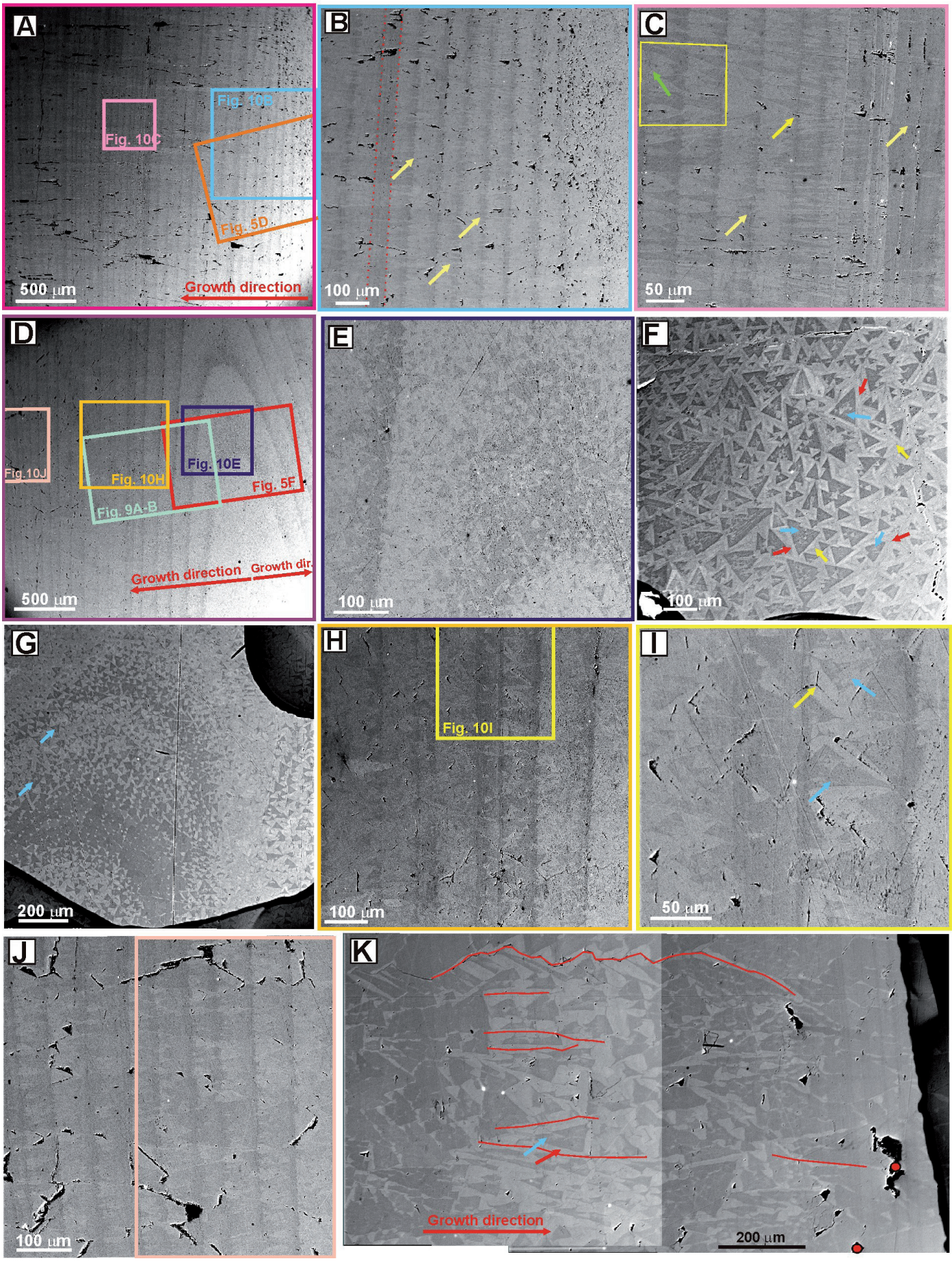
A
Fig. 10C
Fig. 10B
Fig. 5D
500 µm
Growth direction
B
100 µm
C
50 µm
D
Fig.10J
Fig. 10H
Fig. 10E
Fig. 5F
Fig. 9A-B
Growth direction
Growth dir
500 µm
E
100 µm
F
100 µm
G
200 µm
H
Fig. 10I
100 µm
I
50 µm
J
100 µm
K
Growth direction
200 µm

ing to Cölfen and Antonietti (2008), the non-classical crystallization process includes particle-mediated crystallization pathways that involve the mesoscopic transformation of self-assembled, metastable or amorphous precursor particles into nano-particulate superstructures, a notable contrast to classical crystallization, which postulates an ion-by-ion or single molecule attachment to a critical crystal nucleus. These superstructures may have high porosity with organic or foreign-ion inclusions (Cölfen *et al.*, 2005) that may eventually decrease as the boundaries among individual crystalline units are eliminated. Indeed, the fusion of these superstructures leads to apparently single crystalline, iso-oriented structures with a final crystal morphology, which is often indistinguishable from a single crystal that formed by ion-by-ion growth (Cölfen *et al.*, 2005; Meldrum and Cölfen, 2008; Viedma *et al.*, 2013; De Yoreo *et al.*, 2015; Ivanov *et al.*, 2015). In this regard, Cuif *et al.* (2011) emphasized "the impossibility of "classical crystallization" accounting for the properties of the materials that result from the biomineralization process" in each chapter of their book. Specifically, in Fig. 7.42 of their book, these authors reported that the radiating prisms of belemnite rostra show calcite cleavage, equivalent to what was shown in Fig. 3G and 3J, which they described as typical for recrystallized material, and that concentric growth layering is preserved despite the recrystallization. Moreover, these authors noted that "the formation of small clusters of grains following a common orientation may correspond to the early stage of the process that produces the rhombohedral cleavage as the end result" and that "in this process, phase-contrast imaging shows that the organic component is expelled to the exterior of the developing clusters, suggesting fusion of their crystal lattices into broader units". The clusters of nanometer-size grains that were observed by Cuif *et al.* (2011) are much smaller than the micrometer-size, iso-orientated, triangularly shaped and fluorescent sectors that were observed in the studied belemnites (Fig. 8A-D). These micrometer-size triangular sectors may have been formed by smaller sub-units; in fact, some SEM images showed that the external surfaces of the calcite crystals were rough (Fig. 3F), which is a common feature of nano-particulate superstructures that form under non-classical crystallization (e.g., Cölfen *et al.*, 2005; Meldrum and Cölfen, 2008; Viedma *et al.*, 2013).

Moreover, the elongated shapes of the non-fluorescent and light-grey overgrowths (Figs 10C, 11F-G, K) are similar to those of the "sheaf of wheat" structures that were described in synthetic calcites by Domínguez Bella and García Ruiz (1986) and shown in their Figs. 2 and 4. These authors demonstrated experimentally that radially arranged $CaCO_3$ fibers that exhibited non-crystallographic symmetry were built from a set of cleaved calcite rhombohedra that were arranged along their c-axis and behaved as a single crystal. Moreover, these authors observed several types of textures in crystal aggregates with sheaf of wheat morphology, such as concentric banding or serrated profiles and mirror planes that contained the axis of the fiber, which the authors described as similar to those that were observed in travertines by Folk *et al.* (1985), and are also similar to the morphologies that were observed in the light-grey sectors in Figs. 10C, 11F-G and 11J-K.

4.3. Implications for paleoenvironmental interpretations based on geochemical analyses

After accepting the presence of original porosity and subsequent fillings in belemnite rostra, the last question to address is when that filling occurred. The absence of luminescence in the non-fluorescent calcite overgrowths and the lack of significant Fe and Mn contents (Fig. 12 and Table I and Fig. 8 of Benito and Reolid, 2012) suggest that precipitation occurred under oxic conditions and probably prior to burial. When fluids become reduced, calcite easily incorporates Mn^{2+}, which activates calcite luminescence, and Fe^{2+}, which is a quencher of luminescence, into its lattice (e.g., Machel and Burton, 1991; Machel *et al.*, 1991). In fact, according to Benito and Reolid (2012), luminescent and relatively Fe- and Mn-rich calcite precipitates after incipient diagenetic alteration and postdating the fracturing of the studied belemnite rostra. In

Fig. 11.- Photographs of transversal sections of belemnite rostra. A-C. TL, PL and FL images, respectively, of specimen PC-37. Note the radially arranged crystals, which emerge from the apical line and display undulose extinction and concentric growth pattern, which are enhanced under FL. The apical region has a cloudy appearance due to diagenetic alteration. D-E. Detailed images of C and D, respectively. Concentric pattern that display alternating intense and weak FL is easily observable. Radial, long and non-fluorescent sectors that traverse the concentric fluorescent pattern are also observable (white arrows) F. BSEM image of the same specimen. Under BSEM, the radial pattern is more noticeable than the concentric pattern, although the latter is still observable. Concentric pattern is observable as sectors with an overall dark-grey color (brown arrows) and sectors with an overall light-grey color (pink arrows). However a small-scale concentric pattern is also noticeable (see G for details). The radial pattern consists of alternating dark-grey and light-grey elongated sectors and is superimposed onto the concentric patterns. The light-grey sectors (which are non-fluorescent in D) sometimes traverse several concentric layers (white arrows). G. Detailed image of F. The light-grey radial sectors correspond to the non-fluorescent areas in E (white arrows), although some differences are observed between the FL and BSEM images because of the different procedures and accuracies of each technique (see text for explanation). The radial pattern is superimposed onto the thin and relatively largely continuous concentric layers, which display intense FL and a dark-grey color (compare E and G). Some of the light-grey sectors traverse the concentric layers (white arrows) and sometimes display symmetrical shapes (yellow squares) and common V-shaped terminations (green arrows). Additionally, the widths of the dark- and light-grey sectors change in accordance with some concentric layering. H-I. TL and FL images, respectively, of the outer sector of the rostrum PC-45, close to the external wall. Note the concentric and radial patterns, which are observable both under TL and FL, although the concentric pattern is enhanced under FL. J-K. BSEM images of the same specimen as in H and I. Both concentric and radial patterns are observed to be composed of dark-grey or light-grey elongated sectors. In this case, the alternating dark-grey and light-grey radial sectors have a micro-fibrous texture (compare with F and G).

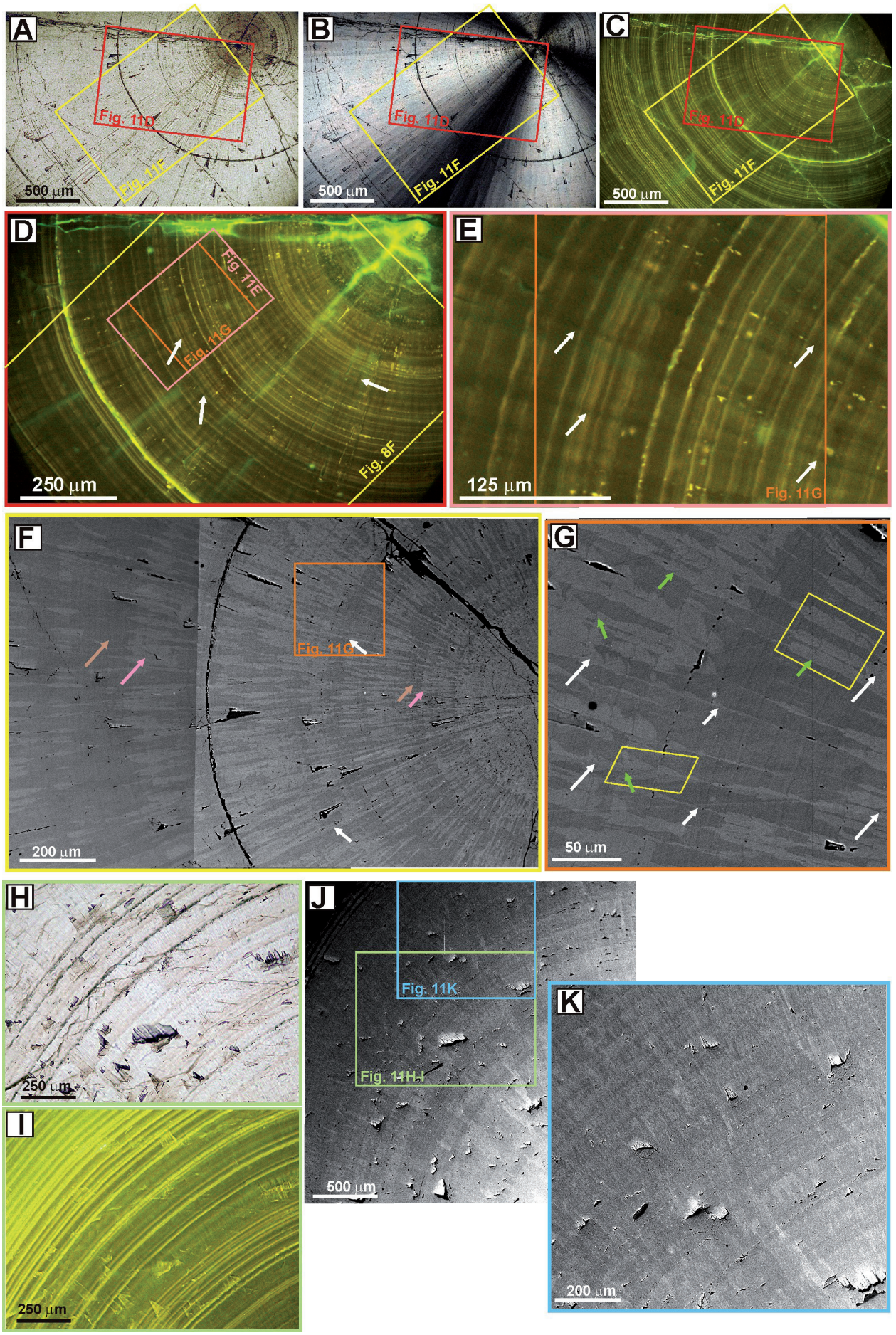
A
Fig. 11D
Fig. 11F
500 μm
B
Fig. 11D
Fig. 11F
500 μm
C
Fig. 11D
Fig. 11F
500 μm
D
Fig. 11E
Fig. 11G
Fig. 8F
250 μm
E
125 μm
Fig. 11G
F
Fig. 11G
200 μm
G
50 μm
H
250 μm
I
250 μm
J
Fig. 11K
Fig. 11H-I
500 μm
K
200 μm

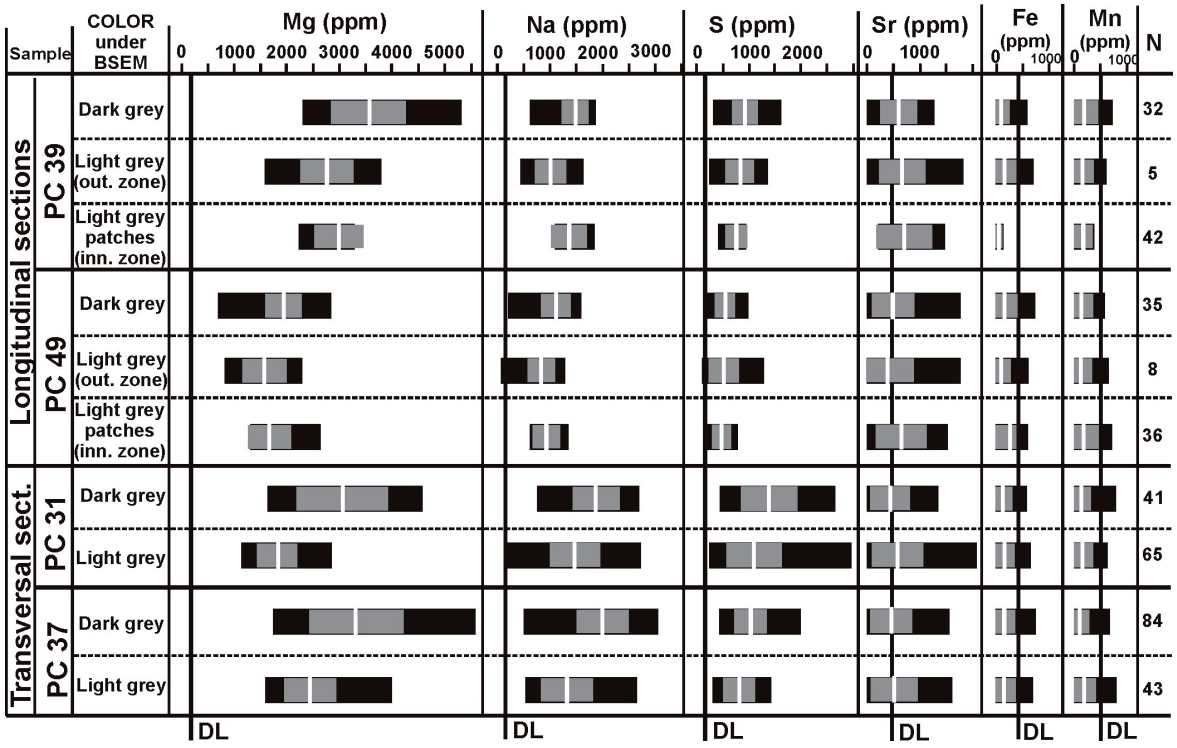

Fig. 12.- Microprobe elemental analyses of the dark-grey and light-grey sectors of the belemnite rostra. The detection limits (DL) are indicated by vertical lines. The horizontal black bars are compositional ranges; the mean values are shown as white vertical bars and the standard deviation as grey horizontal bars. N is the number of elemental analyses (See Fig. 13 for scatter plots of Mg/Na and Mg/S of the forth specimens).

addition, belemnite rostra were bored by endolithic organisms at the seafloor (Reolid and Benito, 2012 and Benito and Reolid, 2012) and our observations indicate that the non-fluorescent calcite precipitated prior to belemnite rostra were bored; in particularly, borings cross-cut both fluorescent and non-fluorescent calcite (Fig. 8I-J). If the pore spaces between the biologically controlled fluorescent calcite were still free when boring occurred, then micrite would have been expected to be present in the pore spaces, which was not observed.

However, another question to address is whether the precipitation of non-fluorescent calcite occurred when the belemnites were still alive or soon after death during the early stages of fossil-diagenesis, prior to their boring and burial. This question has important implications for making paleoenvironmental and/or paleoclimatic interpretations based on geochemical and isotopic analyses of belemnite rostra. Belemnites are considered to be nektonic organisms (Jeletsky, 1966; Spaeth *et al.*; 1971, Richter *et al.*, 2011) that probably migrated laterally and vertically through waters of different temperature and/or salinity during their life cycles, as interpreted by C and O isotopic signatures (Wright, 1987; Sælen *et al.*, 1996). The mean ocean temperature decreases progressively with depth (for example, between 10º and 15º C in the first 500 m at middle latitudes; Locarmini *et al.*, 2010), so the temperature at which the belemnites presumably lived, despite their vertical or lateral variation, may have been warmer or even much warmer than the water temperature at the seafloor, depending on the settling depth after death, thus, the O isotopic composition of the calcite that precipitated at each temperature would be different. Moreover, the shift in isotopic composition could be even larger if it is considered that the O isotopic composition of the seawater became heavier with depth in recent oceans (LeGrande and Schmidt, 2006).

One possibility could be that the precipitation of non-fluorescent calcite occurred while the belemnites were still alive, for example, as a product of a biologically induced mineralization process and not a biologically controlled process (*sensu* Lowenstam and Weiner, 1989 and Mann, 2001). In this sense, Barskov (1973) referenced a distinctive "secondary" calcification process in the middle plate of the shield of modern *Sepia* specimens. According to this author, "secondary calcification" occurs "without contact with the epithelium, and after the middle plate after this layer has been isolated from the epithelial cells which secrete it" and "by means of the chamber fluid between the chambers of the swelling", which would be the "supplier of the calcium ions, carbonate ions and, probably enzymes responsible for calcification". The precipitation of non-fluorescent calcite overgrowths while the belemnites were alive would have probably modified the rostrum density and, as Spaeth (1975) suggested, their buoyancy and gravity centers, making them too heavy to support the swimming animal's horizontal living posture.

The other possibility is that the non-fluorescent calcite overgrowths precipitated after the death of the belemnites at the oxidized seafloor because they are non-luminescent and do not contain significant amounts of Fe and Mn. Moreover, the precipitation of overgrowths likely occurred very rapidly because they formed prior to boring by endolithic organisms.

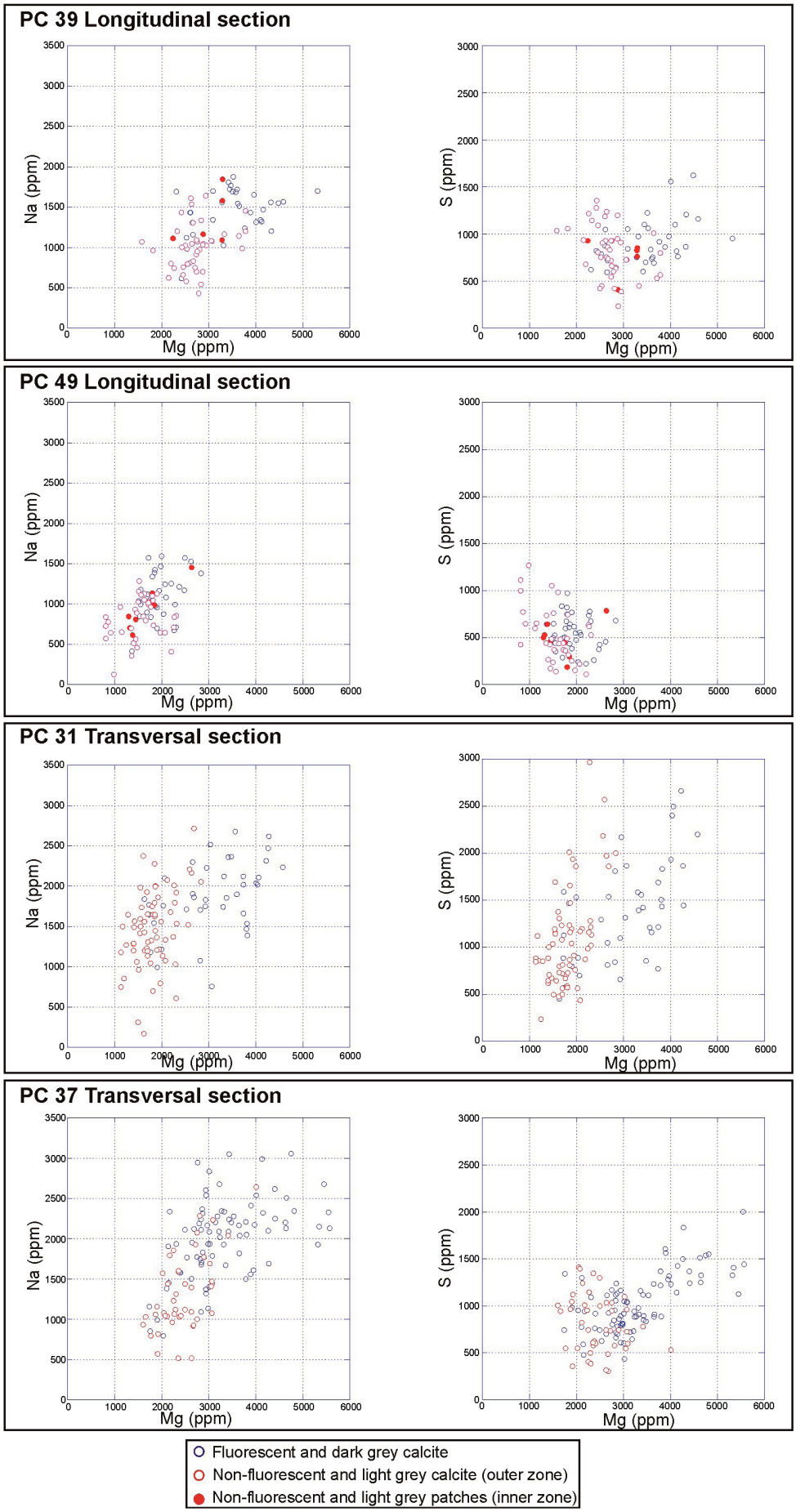

Fig. 13.- Scatter plots diagrams showing Mg/Na and Mg/S correlation (in ppm) of the same samples than those analyzed in Fig. 12. Note that fluorescent and dark-grey calcite (in blue color) have overall higher Mg and Na content than non-fluorescent and light-grey calcite (in red color), both of the outer zone and the patches of the inner zone. S contents of fluorescent and dark-grey calcite are similar than those obtained in non-fluorescent and light-grey calcite in most samples although mean values are slightly higher in dark-grey calcite (see Fig. 12 for mean values and standard deviations).

In this regard, these crystals, which exhibited reentrant angles in the crystallographic direction, such as the V-shape terminations that were observed in the non-fluorescent and light-grey calcite sectors (Figs. 10C and 11G), often showed elongated morphology because of the enhanced growth rate in the crystallographic direction of the reentrant angle, such as in twinned crystals (Kitamura *et al.*, 1979; Otálora and García-Ruiz, 2014).

Researchers should be able to confirm that calcite overgrowths would have different petrographic and geochemical features depending on the diagenetic environment under which they precipitated (i.e., oxic, as in the studied rostra, sub-oxic or reduced) to corroborate the hypothesis that calcite overgrowths precipitate after the death of belemnites. In this regard, petrographic observations that were made on poorly preserved belemnite rostra by Richter *et al.* (2003) and Benito and Reolid (2012) indicated that calcite overgrowths precipitated under sub-oxic or even reduced conditions because they are luminescent and contained significant amounts of Fe and Mn, reinforcing the hypothesis that the belemnite rostra were originally porous and that the calcite overgrowths precipitated once the belemnites died.

Several authors have observed intra- and inter-specimen changes in the isotopic values of belemnite rostra (e.g. Sælen *et al.*, 1996; Price and Sellwood, 1997; Podhala *et al.*, 1998; Rosales *et al.*, 2001; Dutton *et al.*, 2007; McArthur *et al.*, 2004, 2007a; Wierzbowski and Joachimski, 2009; Benito and Reolid, 2012). Differences in the $\delta^{18}O$ values within a single belemnite have been interpreted by these authors as a reflection of the variability of seawater temperature during belemnite growth, if it is assumed that belemnite migrated laterally and vertically through seawater at different temperatures, and that calcite precipitated in oxygen isotope equilibrium with ambient seawater. However, if belemnites were originally porous it is plausible that intra- and inter-specimen changes of $\delta^{18}O$ values could be a reflection of analyzing concentric areas of the rostrum having different proportion of fluorescent and biologically controlled calcite and non-fluorescent calcite precipitated subsequently as overgrowths. This question could be addressed in further studies, for example, by performing separate isotopic analyses in concentric layers with either more or less intense fluorescence, to confirm if the carbon and/or oxygen isotopic composition changes in accordance with changes in the fluorescence of the concentric layering.

5. Conclusions

The calcite crystals in the rostrum solidum of Jurassic belemnites grew from spherulites that successively developed along the apical line, resulting in a "regular spherulithic prismatic" microstructure. Radially arranged crystals emerged and diverged from the spherulites towards the apex and the external walls of the rostrum, progressively increasing their length and thickness and becoming prismatic.

Concentric growth pattern is observed at different scales from around 1 μm to dozens of microns, with the layers displaying alternating intense or weak FL. The concentric pattern is superimposed and traversed by a radial pattern, which is noticeable under TL, FL and BSEM, and create the microfibrous texture in the rostra's calcite crystals. The radial sectors change their shape and width as successive concentric layers are formed, which suggests that the growth of the belemnite rostra was not continuous.

Single calcite crystals are composite and formed during two different growth stages under different circumstances, which strongly suggest that the belemnite rostra were originally porous. Single crystals consistently comprise an inner zone or sector, which is fluorescent, has relatively high Mg, Na and S contents, and is interpreted to be a product of biologically controlled mineralization during belemnite growth, and an outer sector, in optical continuity, which is non-fluorescent, has relatively low Mg, Na and S contents, and is interpreted to have precipitated as overgrowths of the former, filling intra- and inter-skeletal porosity.

The precipitation of calcite overgrowths occurred very rapidly under oxic conditions before burial and prior to boring by endolithic organisms, which could have important implications for making paleoenvironmental and/or paleoclimatic interpretations based on geochemical and isotopic analyses of belemnite rostra.

The composite nature of the crystals at various scales reinforces the hypothesis of other authors that non-classical crystalization processes occur during the formation of belemnite rostra.

Acknowledgements

This research was carried out with the financial support of the projects CGL2011-22709, CGL2014-52670-P and RYC-2009-04316 (Ramón y Cajal Program, Ministerio de Ciencia e Innovación), and by the "Sedimentary Basin Analysis" and "Paleoclimatology and Global Change" research groups of the Complutense University of Madrid. The manuscript greatly benefited from comments by several reviewers since it was written in March 2016. In particular we apprecieate the suggestions by Dr. Gunnar Sælen and Dr. Jacinto Alonso-Azcárate, that really improve the manuscript. We are also thankful to Sonia Campos for field assistance, to for its critical review, to Antonio Piedra, Beatriz Moral, Aitor Antón and Juan Carlos Salamanca for thin-sections preparation, to Alfredo Larios and Xabier Arroyo for their technical assistance with microprobe and scanning electron microscopy, and to Laura Donadeo and María Victoria Romero for their help with bibliography. The paper was edited by Elsevier Language Editing Services.

Critical reviews stimulate scientific progress, leading to better papers by the authors. Manuscripts also can inspire reviewers research, which can be also good for the science, as long as they keep within the expected ethical behavior.

References

Alberti, M., Fürsich, F.T., Pandey, D.K. (2012): The Oxfordian stable isotope record ($\delta^{18}O$, $\delta^{13}C$) of belemnites, brachiopods, and oysters from the Kachchh Basin (western India) and its potential for palaeoecologic, palaeoclimatic and palaeogeographic reconstructions. *Palaeogeography, Palaeoclimatology, Palaeoecology* 344-345, 49-68. doi:10.1016/j.palaeo.2012.05.018

Anderson, T.F., Popp, B.N., Williams, A.C., Ho, L.-Z., Hudson, J.D. (1994): The stable isotopic records of fossils from the Peterborough Member, Oxford Clay Formation (Jurassic), UK: palaeoenvironmental implications. *Journal of the Geological Society of London* 151, 125-138. doi: 10.1144/gsjgs.151.1.0125

Armendáriz, M., Rosales, I., Bádenas, B., Aurell, M., García-Ramos, J.C., Piñuela, L. (2012): High-resolution chemostratigraphic records from Lower Pliensbachian belemnites: Palaeoclimatic perturbations, organic facies and water mass exchange (Asturian basin, northern Spain). *Palaeogeography, Palaeoclimatology, Palaeoecology* 333-334, 178-191. doi:10.1016/j.palaeo.2012.03.029

Arkhipkin, A.I., Bizikov, V.A., Fuchs, D. (2012): Vestigial phragmoconoe in the gladius points to a deepwater origin of squid (Mollusca: Cephalopoda). *Deep-Sea Research I* 61, 109-122. doi:10.1016/j.dsr.2011.11.10

Bailey T.R., Rosenthal Y., McArthur J.M., Van de Schootbrugge B., Thirlwall M.F. (2003): Paleoceanographic changes of the Late Pliensbachian–Early Toarcian interval: a possible link to the genesis of an Oceanic Anoxic Event. *Earth and Planetary Science Letters* 212, 307-320. doi:10.1016/S0012-821X(03)00278-4

Bandel, K., Engeser, T, Reitner, J. (1984): Die Embryonal Entwicklung von *Hibolithes* (Be1emnitida, Cephalopoda). Neues Jahrbuch für Geologie und Paläontologie Abhandlungen 167, 275-303.

Bandel, K, Spaeth, C. (1988): Structural differences in the ontogeny of some belemnite rostra. In: Wiedmann, J, Kullimann, J. (Eds.), *Cephalopods-Present and Past*, Schweizerbart'sche Vcrlagsbuchhandlung. Stuttgart, pp. 247-271.

Barskov, I.S. (1970): Structure of the belemnitid rostrum. *Paleontological Journal* 4, 110-112.

Barskov; I.S. (1973): Microstructure of the skeletal layers of *Sepia* and *Spirula* compared with the shell layers of other mollusks. *Paleontological Journal* 7, 285-294.

Bathurst, R.G.C. (1975): *Carbonate sediments and their diagenesis*, Amsterdam, Elsevier, 658 pp.

Benito, M.I., Reolid, M. (2012): Belemnite taphonomy (Upper Jurassic, Western Tethys) part II: Fossil-diagenetic analysis including combined petrographic and geochemical techniques. *Palaeogeography, Palaeoclimatology, Palaeoecology* 358-360, 89-108. doi:10.1016/j.palaeo.2012.06.035.

Benito, M.I., Reolid, M., Campos-Soto, S. (2014): Comparisons between Belemnitida and Sepiida: Is the cuttlebone prong an analogue of the belemnite rostrum?. In: Klug, C and Fuchs, D.(eds), *Cephalopods - Present and Past 9 & Coleoids through Time 5*. Palaontologisches lnstitut und Museum, Universitat Zürich, p. 103.

Boto, K., Isdale, P.J. (1985): Fluorescent bands in massive corals result from terrestrial fulvic acid inputs to the nearshore zone. *Nature* 315, 396-397. doi:10.1038/315396a0

Busenberg, E., Plummer, I.N. (1985): Kinetic and thermodynamic factors controlling the distribution of SO_3^{-2} and Na^+ in calcites and selected aragonites. *Geochimica et Cosmochimica Acta* 49, 713-725. doi:10.1016/0016-7037(85)90166-8

Carter, J.G., Clark, II, G.R. (1985): Classification and phylogenetic significance of molluscan shell microstructure. In: Bottjer, D.J., Hickman, C.S., Ward, P.D. (eds.), *Mollusks. Notes for a short course*. University of Tennessee Department of Geological Sciences Studies in Geology 13, 50-71.

Cercone, K.R., Dembski, H., Pedone, V.A. (1985): Fluorescence of carbonates: evidence that growth zoning can be caused by dispersed organic matter. *Geological Society of America, Abstract with Program*, p. 541.

Coimbra, R., Olóriz, F. (2012): Pixel counting for percentage estimation: applications to sedimentary petrology. *Computers & Geosciences* 42, 212–216. doi: 10.1016/j.cageo.2011.10.014.

Clark, G.R., II (1999): Organic matrix taphonomy in some molluscan shell microstructures. *Palaeogeography, Palaeoclimatology, Palaeoecology* 149, 305-312. doi:10.1016/S0031-0182(98)00208-9

Clark, G.R., II (2005): Organic matrix in the porifera and cnidaria: déjà vu through a temporal telescope. *Geological Society of America, Abstracts with Programs* 37, p. 366.

Cölfen, H., Antonietti, M. (2005): Mesocrystals: Inorganic superstructures made by highly parallel crystallization and controlled aligment. *Angewandte Chemie International Edition* 44, 5576-5591. doi:10.1002/anie.200500496

Cölfen, H., Antonietti, M. (2008): *Mesocrystals and non-classical mineralization.* Jhon Wiley & Sons, Ltd, England 276 pp.

Cuif, J.P., Dauphin, Y., Sorauf, J.E. (2011): *Biominerals and fossils through time*. Cambridge University Press, UK. 490 pp.

Dauphin, Y., Williams, C.T., Barskov, I.S. (2007): Aragonitic rostra of the Turonian belemnitid *Goniocamax*: arguments from diagenesis. *Acta Palaeontologica Polonica* 52, 85-97.

De Yoreo, J.J., Gilbert, P.U.P.A., Sommerdijk, N.A.J.M., Penn, R.L., Whitelam, S., Joester, D., Zhang, H., Rimer, J.D., Navrotsky, A., Banfield, J.F., Wallace, A.F., Michel, F.M., Meldrum, F.C., Cölfen, H., Dove, P.M. (2015): Crystallization by particle attachment in synthetic, biogenic, and geologic environments. *Science* 349(6247), aaa6760-1-aaa6760-9. doi:10.1126/science.aaa6760

Domínguez Bella, S., García-Ruiz, J.M. (1986): Textures in induced morphology crystal aggregates of CaCO3: Sheaf of wheat morphologies. *Journal of Crystal Growth* 79, 236-240.

Dunca, E., Doguzhaeva, L., Schöne, B.R., Schootbrugge, B. (2006): Growth patterns in rostra of the Middle Jurassic belemnite *Megateuthis giganteus*: controlled by the moon? *Acta Universitatis Carolinae – Geologica* 49, 107-117.

Dutton, A., Huber, B.T., Lohmann, K.C., Zinsmeister, W.J. (2007): High-resolution stable isotope profiles of a dimitobelid belemnite: implications for paleodepth habitat and Late Maastrichtian climate seasonality. *Palaios* 22, 642-650. doi:10.2110/palo.2005.p05-064r

Florek, M., Youn, H.S., Ro, C.-U., Wierzbowski, H., Osán, J., Kazimierczak, W., Kuczumow (2004): Investigation of chemical composition of belemnite rostra by synchroton based X-ray microfluorescence and diffraction and electron microprobe. *Journal of Alloys and Compounds* 362, 99-106. doi:10.1016/S0925-8388(03)00569-3

Folk, R.L. (1965): Some aspect of recrystallization of ancient limestones. In: Pray, L.C., Murray, R.C. (Eds.), *Dolomitization and Limestone Diagenesis: a symposium. SEPM Special Publication* 13, 14-48.

Gómez J.J., Goy A., Canales M.L. (2008): Seawater temperature and carbon isotope variations in belemnites linked to mass extinction during the Toarcian (Early Jurassic) in Central and Northern Spain. Comparison with other European sections. *Palaeogeography, Palaeoclimatology, Palaeoecology* 258, 28-58. doi:10.1016/j.palaeo.2007.11.005

Gómez J.J., Goy A. (2011): Warming-driven mass extinction in the Early Toarcian (Early Jurassic) of northern and central Spain. Correlation with other time-eqivalent European sections. *Palaeogeography, Palaeoclimatology, Palaeoecology* 306, 176-195. doi:10.1016/j.palaeo.2011.04.018

Ivanov, V.K., Fedorov, P.P., Baranchikov, A.Ye., Osiko, V.V. (2015): Oriented attachment of particles: 100 years of investigations of non-classical crystal growth. *Russian Chemical Reviews* 83, 1204-1222.

Jelesky, J.A. (1966): Comparative morphology, phylogeny, and classification of fossil Coleoidea. Mollusca, Article 7. *Paleontological Con-*

tributions. University of Kansas, 1-162.

Kitamura, M., Hosoya, S., Sunagawa, I. (1979): Re-investigation of the re-entrant corner effect in twinned crystals. Journal of Crystal Growth 47, 93-99. doi:10.1016/0022-0248(79)90162-3

LeGrande, A.N., Schmidt, G.A. (2006): Global gridded data set of the oxygen isotopic composition in seawater. *Geophysical Research Letters* 33, L12604, 1-5. doi:10.1029/2006GL026011.

Li, Q., McArthur, J.M., Atkinson, T.C. (2012): Lower Jurassic belemnites as indicators of palaeo-temperature. *Palaeogeography, Palaeoclimatology, Palaeoecology* 315-316, 38-45. doi:10.1016/j. palaeo.2011.11.006

Locarnini, R.A., Mishonov ,A.V., Antonov, J.I., Boyer, T.P., García, H.E., Baranova, O.K., Zweng, M.M., Johnson, D.R. (2010): World Ocean Atlas 2009, Volume 1: Temperature. Levitus, S. (Ed.). NOAA Atlas NESDIS 68, U.S. Government Printing Office, Washington, D.C., 184 pp.

Lowenstam, H.A., Weiner, S. (1989): *On biomineralization*. Oxford University Press. New York. USA. 324 pp.

McArthur, J.M., Donovan, D.T., Thirlwall, M.F., Fouke, B.W., Mattey, D. (2000): Strontium isotope profile of the early Toarcian (Jurassic) ocean anoxic event, the duration of ammonite biozones, and belemnite palaeotemperatures. *Earth and Planetary Science Letters* 179, 269-285. doi:10.1016/S0012-821X(00)00111-4

McArthur, J.M., Mutterlose, J., Price, G.D., Rawson, P.F., Ruffel, A., Thirlwall, M.F. (2004): Belemnites of Valanginian, Hauterivian and Barremian age: Sr isotope stratigraphy, composition ($^{87}Sr/^{86}Sr$, ^{13}C, ^{18}O, Na, Sr, Mg), and palaeooceanography. *Palaeogeography, Palaeoclimatology, Palaeoecology* 202, 253-272. doi:10.1016/S0031-0182(03)00638-2

McArthur, J.M., Doyle, P., Leng, M.J., Reeves, K., Williams, C.T., García-Sánchez, R., Howarth, R.J. (2007): Testing palaeo-environmental proxies in Jurassic belemnites: Mg/Ca, Sr/Ca, Na/Ca, $\delta^{18}O$ and $\delta^{13}C$. *Palaeogeography, Palaeoclimatology, Palaeoecology* 252, 464-480. doi:10.1016/j.palaeo.2007.05.006

Machel, H.G., Burton, E. (1991): Factors Governing Cathodoluminescence in Calcite and Dolomite and their Implications for Studies of Carbonate Diagenesis. In: Barker, C.E., Kopp, O.C. (eds.), *Luminiscence microscopy and Spectroscopy: Qualitative and Quantitative Applications. SEPM Short Course* 25, 37-58.

Machel, H.G., Mason, R.A., Mariano, A.N., Mucci, A. (1991): Causes and Measurements of Luminescence in Calcite and Dolomite. In: Barker, C.E., Kopp, O.C. (eds.), *Luminiscence microscopy and Spectroscopy: Qualitative and Quantitative Applications. SEPM Short Course* 25, 9-25.

Mann, S. (2001): *Principles and concepts in bioinorganic materials chemistry*. Oxford University Press. Oxford, UK. 198 pp.

Marin, F., Narayanappa, P., Motreuil, S. (2001): Acidic Shell proteins of the mediterranean fan mussel *Pinna nobilis*. In: Müller, W.E.G. (ed.), *Molecular biomineralization: Aquatic organisms forming extraordinary materials. Progress in molecular and subcellular biology: Marine molecular biotechnology* 52. Springer. Heidelberg, Germany, pp. 353-395.

Meldrum, F.C., Cölfen, H. (2008): Controlling mineral morphologies and structures in biological and synthetic systems. *Chemical Reviews* 108, 4332-4432. doi:10.1021/cr8002856

Müller-Stoll, H. (1936): Beitrage zur Anatomie der Belemnoidea. *Nova Acta Leopoldina Neue Serie* 4, 159-226.

Niebuhr, B., Joachimski, M.M. (2002): Stable isotope and trace element geochemistry of Upper Cretaceous carbonates and belemnite rostra (Middle Campanian, north Germany). *Geobios* 35, 51-64. doi:10.1016/S0016-6995(02)00009-8

Nieto, L.M., Ruiz-Ortiz, P.A., Rey, J., Benito, M.I. (2008): Sr-Isotope Stratigraphy (SIS) elucidates the age of condensed levels: Examples from the Subbetic (Southern Spain). *Sedimentology* 55, 1-29. doi:10.1111/j.1365-3091.2007.00891.x

Nunn, E.V., Price, G.D. (2010): Late Jurassic (Kimmeridgian-Tithonian) stable isotopes ($\delta^{18}O$, $\delta^{13}C$) and Mg/Ca ratios: new palaeoclimate data from Helmsdale, northeast Scotland. *Palaeogeography*, *Palaeoclimatology*, *Palaeoecology* 292, 325-335. **doi:** 10.1016/j.palaeo.2010.04.015

Nunn, E.V., Price, G.D., Hart, M.B., Page, K.N., Leng, M.J. (2009): Isotopic signals from Callovian-Kimmeridgian (Middle-Upper Jurassic) belemnite and bulk organic carbon, Staffin Bay, Isle of Skye, Scotland. *Journal Geological Society London* 166, 633-641. doi:10.1144/0016-76492008-067.

Olóriz, F., Reolid, M., Rodríguez-Tovar, 869 F.J. (2002). Fossil assemblages, lithofacies and taphofacies for interpreting depositional dynamics in the epicontinental Oxfordian of the Prebetic Zone, Betic Cordillera, southern Spain. *Palaeogeography, Palaeoclimatology, Palaeoecology* 185, 53–75.

Olóriz, F., Reolid, M., Rodríguez-Tovar, F.J. (2012). Palaeogeography and relative sea-level history forcing eco-sedimentary contexts in Late Jurassic epicontinental shelves (Prebetic Zone, Betic Cordillera): an ecostratigraphic approach. *Earth-Science Reviews* 111, 154-178. doi: 10.1016/j.earscirev.2011.11.004.

Otálora, F., García-Ruiz, J.M. (2014): Nucleation and growth of the Naica giant gypsum crystals. *Chemical Society Reviews* 43, 1999-2374. doi:10.1039/C3CS60320B

O'Neil, B.R., Manger, W.L., Hays, P.D. (2003): Growth and diagenesis of middle Jurassic belemnite rostra from northeastern Utah: insights using cathodoluminescence. In: Warnke, K., Keupp, H, Boletzky, S. (eds.), *Coleoid cephalopods through time. Berliner Paläobiologische Abhandlungen* 3, 241-251.

Pedone, V.A., Cercone, K.R., Burrus, R.C. (1990): Activators of photoluminescence in calcite: evidence from high resolution, laser-excited luminescence spectroscopy. *Chemical Geology* 88, 183-190. doi:10.1016/0009-2541(90)90112-k

Pingitore, N.E., Jr., Meitzner, G., Love, K.M. (1995): Identification of sulfate in natural carbonates by X-ray absorption spectroscopy. *Geochimica et Cosmochimica Acta* 59, 2477-2483. doi:10.1016/0016-7073(95)00142-5

Podhala, O.G., Mutterlose, J., Veizer, J. (1998): Preservation of $\delta^{18}O$ and $\delta^{13}C$ in belemnite rostra from the Jurassic/Early Cretaceous successions. *American Journal of Sciences* 298, 324-347. doi:10.2475/ajs.298.4.324

Price, G.D., Gröcke, D.R. (2002): Strontium-isotope stratigraphy and oxygen- and carbon-isotope variation during the Middle Jurassic-Early Cretaceous of the Falkland Plateau, South Atlantic. *Palaeogeography, Palaeoclimatology, Palaeoecology* 183, 209-222. doi:10.1016/S0031-0182(01)00486-2

Price, G.D., Rogov, M.A. (2009): An isotopic appraisal of the Late Jurassic greenhouse phase in the Russian Platform. *Palaeogeography Palaeoclimatology Palaeoecology* 273, 41-49. doi:10.1016/j.palaeo.2008.11.011

Price, G.D., Sellwood, B.W. (1994): Palaeotemperatures indicated by Upper Jurassic (Kimmeridgian-Tithonian) fossils from Mallorca determined by oxygen isotope composition. *Palaeogeography, Palaeoclimatology, Palaeoecology* 110, 1-10. doi:10.1016/0031-0182(94)90106-6

Price, G.D., Sellwood, B.W. (1997): "Warm" palaeotemperatures from high Late Jurassic palaeolatitudes (Falkland Plateau): Ecological, environmental or diagenetic controls? *Palaeogeography, Palaeoclimatology, Palaeoecology* 129, 315-327. doi:10.1016/S0031-0182(96)00058-2

Prokoph, A., Shields, G.A., Veizer, J. (2008): Compilation and time-series analysis of a marine carbonate $\delta^{18}O$, $\delta^{13}C$, $^{87}Sr/^{86}Sr$ and $\delta^{34}S$

database through Earth history. *Earth-Science Reviews* 87, 113-133. doi:10.1016/j.earscirev.2007.12.003

Reolid, M., Benito, M.I. (2012): Belemnite taphonomy (Upper Jurassic, Western Tethys) Part I: biostratinomy. *Palaeogeography, Palaeoclimatology, Palaeoecology* 358-360, 72-88. doi:10.1016/j.palaeo.2012.06.012

Richter, D., Götte, T., Götze, J., Nauser, R.D. (2003): Progress in application of cathodoluminescence (CL) in sedimentary petrology. *Mineralogy and Petrology* 79, 127-166. doi:10-1007/s00711-003-0237-4

Richter, D., Nauser, R.D., Schreuer, J., Gies, H., Imenhauser, A. (2011): Radiaxial-fibrous calcites: A new look at an old problem. *Sedimentary Geology* 239, 23-36. doi:10.1016/j.sedgeo.2011.06.004

Rosales, I., Quesada, S., Robles, S. (2001): Primary and diagenetic isotopic signal in fossils and hemipelagic carbonates: the Lower Jurassic of northern Spain. *Sedimentology* 48, 1149-1169. doi:10.1046/j.1365-3091.2001.00412

Rosales, I., Quesada, S., Robles, S. (2004a): Paleotemperature variations of Early Jurassic seawater recorded in geochemical trends of belemnites from the Basque-Cantabrian basin, northern Spain. *Palaeogeography, Palaeoclimatology, Palaeoecology* 203, 253-275. doi:10.1016/S0031-0182(03)00686-2

Rosales, I., Robles, S., Quesada, S. (2004b): Elemental and oxygen isotope composition of Early Jurassic belemnites: salinity vs. temperature signals. *Journal of Sedimentary Research* 74, 342-354. doi:10.1306/112693740342

Sabatini, D.D., Miller, F., Barrnett, R.J. (1964): Aldehyde fixation for morphological and enzyme histochemical studies with the electron microscope. *Journal of Histochemistry & Cytochemistry* 12, 57-71.

Sælen, G. (1989): Diagenesis and construction of the belemnite rostrum. *Palaeontology* 32, 765-798.

Sælen, G., Karstang, T.V. (1989): Chemical signatures of belemnites. *Neues Jahrbuch für Geologie und Paläontologie Abhandlungen* 177, 333-346.

Sælen, G., Doyle, P., Talbot, M.R. (1996): Stable-isotope analyses of belemnite rostra from the Whitby Mudstone Fm., England: Surface water conditions during deposition of a marine black shale. *Palaios* 11, 97-117. doi:10.2307/3515065

Spaeth, C.H.R. (1971): Aragonitische und calcitische primär-strukturen im Schalenbau eines Belemniten aus der englischen Unterkreide. *Paläontologische Zeitschrift* 45, 33-40.

Spaeth, C.H.R. (1973): Weitere Untersuchungen der Primär- und Fremdstrukturen in calcitischen und aragonitischen Schalenlagen englischer Unterkreide-Belemniten. *Paläontologische Zeitschrift* 47, 163-174.

Spaeth, C.H.R. (1975): Zur Frage der Schwimmverhältnisse bei Belemniten in Abhängigkeit vom Primärgefüge der Hartteile. *Paläontologische Zeitschrift* 49, 321-331.

Spaeth, C.H.R., Hoefs, J., Vetter, U. (1971): Some aspects of isotopic composition of belemnites and related paleotemperatures. *Geological Society of America Bulletin* 82, 3139-3150. doi:10.1130/0016-7606(1971)82[3139:SAOICO]2.0.CO:2

Stevens, G.R., Clayton, R.N. (1971): Oxygen isotope studies on Jurassic and Cretaceous belemnites from New Zealand and their biogeographic significance. *New Zealand Journal of Geology and Geophysics* 14, 829-887.

Sturz-Köwing, I. (1960): Veränderungen im Inneren von Belemnitenrostren des oberen Lias. *Schriften des Naturwissenschaftilichen Vereins für Scheleswing-Holstein* 30,60-67.

Ullmann, C.V., Frei, R., Korte, C., Hesselbo, S.P. (2015): Chemical and isotopic architecture of the belemnite rostrum. *Geochimica et Cosmochimica Acta* 159, 231-243. doi:10.1016/J.GCA.2015.03.034

Veizer, J. (1974): Chemical diagenesis of belemnite shells and possible consequences for paleotemperature determinations. *Neues Jahrbuch Geologie Paläontologie Abhandlungen* 147, 91-111.

Veizer, J., Fritz, P. (1976): Possible control of post-depositional alteration in oxygen paleotemperature determinations. *Earth and Planetary Science Letters* 33, 255-260. doi:10.1016/0012-821X(76)90232-6

Veizer, J., Prokoph, A. (2015): Temperatures and oxygen isotopic composition of Phanerozoic oceans. *Earth-Science Reviews* 146, 92-104. doi:10.1016/j.earscirev.2015.03.008

Veizer, J., Ala, D., Azmy, K., Bruckschen, P., Buhl, D., Bruhn, F., Carden, G.A.F., Diener, A., Ebneth, S., Godderis, Y., Jasper, T., Korte, C, Pawellek, F., Podlaha, O.G., Strauss, H. (1999): $^{87}Sr/^{86}Sr$, $\delta^{13}C$ and $\delta^{18}O$ evolution of Phanerozoic seawater. *Chemical Geology* 161, 59-88. doi:10.1016/S0009-2541(99)00081-9

Viedma, C., McBride, J.M., Kahr, B., Cintas, P. (2013): Enantiomer-specific oriented attachment: formation of macroscopic homochiral crystal aggregates from a racemic system. *Angewandte Chemie International Edition* 52, 10545-10548. doi:10.1002/anie.201303915

Westbroek, P., Van der Meide, P.H., Van der Wey-Kloppers, J.S., Van der Sluis, R.J., De Leeuw, J.W., de Jong, E.W. (1979): Fossil macromolecules from cephalopod shells: characterization, immunological response and diagenesis. *Paleobiology* 5, 151-167.

Wierzbowski, H. (2004): Carbon and oxygen isotope composition of Oxfordian-Early Kimmeridgian belemnite rostra: palaeoenvironmental implications for Late Jurassic seas. *Palaeogeography, Palaeoclimatology, Palaeoecology* 203, 153-168. doi:10.1016/S0031-0182(03)00673-4

Wierzbowski, H., 2013. Life span and growth rate of Middle Jurassic mesohibolitid belemnites deduced from rostrum microincrements. Volumina Jurassica 11, 1–18.

Wierzbowski, H., Joachimski, M.M. (2007): Reconstruction of late Bajocian-Bathonian marine palaeoenvironments using carbon and oxygen isotope ratios of calcareous fossils from the Polish Jura Chain (central Poland). *Palaeogeography, Palaeoclimatology, Palaeoecology* 254, 523-540. doi:10.1016/j.palaeo.2007.07.010

Wierzbowski, H., Joachimski, M.M. (2009): Stable isotopes, elemental distribution, and growth rings of belemnopsid belemnite rostra: proxies for belemnite life habitat. *Palaios* 24, 377-386. doi:10.2110/palo.2008.p08-101r

Wierzbowski, H., Rogov, M. (2011): Reconstructing the palaeoenvironment of the Middle Russian Sea during the Middle–Late Jurassic transition using stable isotope ratios of cephalopod shells and variations in faunal assemblages. *Palaeogeography, Palaeoclimatology, Palaeoecology* 299, 250-264. doi:10.1016/j.palaeo.2010.11.006

Wierzbowski, H., Dembicz, K., Praszkier, T. (2009): Oxygen and carbon isotope composition of Callovian-Lower Oxfordian (Middle-Upper Jurassic) belemnite rostra from central Poland: A record of a Late Callovian global sea-level rise? *Palaeogeography Palaeoclimatology Palaeoecology* 283, 182-194. doi:10.1016/j.palaeo.2009.09.020

Wright, E.K. (1987): Stratification and paleocirculation of the Late Cretaceous Western Interior Seaway of North America. *Geological Society of America Bulletin* 99, 480-490. doi:10.1130/0016-7606(1987)99<480:SAPOTL>2.0.CO;2

Appendix: Belemnite samples

Table 1.- Table showing the genera of each belemnite specimen analyzed including the lithofacies and the stratigraphic position where they were collected. Specimens named with NEW correspond to the 10 new samples collected after Benito and Reolid (2012).

Specimen name	Genus	Preservation	Ammonite biozone	Lithofacies
PC-02-44	*Hibolithes*	Non-altered	Transversarium Zone, Middle Oxfordian	Spongiolithic limestone
PC-04-02	*Hibolithes*	Non-altered	Transversarium Zone, Middle Oxfordian	Spongiolithic limestone
PC-04-28	*Belemnopsis*	Non-altered	Transversarium Zone, Middle Oxfordian	Spongiolithic limestone
PC-05-107	*Hibolithes*	Non-altered	Transversarium Zone, Middle Oxfordian	Spongiolithic limestone
PC-05-20		Partially altered	Transversarium Zone, Middle Oxfordian	Spongiolithic limestone
PC-05-03		Non-altered	Transversarium Zone, Middle Oxfordian	Spongiolithic limestone
PC-06-23B		Partially altered	Transversarium Zone, Middle Oxfordian	Spongiolithic limestone
PC-08	*Hibolithes*	Non-altered	Transversarium Zone, Middle Oxfordian	Spongiolithic limestone
PC-08-31		Non-altered	Transversarium Zone, Middle Oxfordian	Spongiolithic limestone
PC-09-02	*Hibolithes*	Partially altered	Transversarium Zone, Middle Oxfordian	Spongiolithic limestone
PC-09-03	*Belemnopsis*	Partially altered	Transversarium Zone, Middle Oxfordian	Spongiolithic limestone
PC-09-05	*Belemnopsis*	Non-altered	Transversarium Zone, Middle Oxfordian	Spongiolithic limestone
PC-10-01	*Hibolithes*	Partially altered	Transversarium Zone, Middle Oxfordian	Spongiolithic limestone
PC-10-04		Non-altered	Transversarium Zone, Middle Oxfordian	Spongiolithic limestone
PC-11-183	*Hibolithes*	Non-altered	Transversarium Zone, Middle Oxfordian	Spongiolithic limestone
PC-11-41	*Belemnopsis*	Non-altered	Transversarium Zone, Middle Oxfordian	Spongiolithic limestone
PC-12-13	*Hibolithes*	Non-altered	Transversarium Zone, Middle Oxfordian	Spongiolithic limestone
PC-13-11		Partially altered	Transversarium Zone, Middle Oxfordian	Spongiolithic limestone
PC-14-45	*Hibolithes*	Non-altered	Transversarium Zone, Middle Oxfordian	Spongiolithic limestone
PC-14-131	*Hibolithes*	Non-altered	Transversarium Zone, Middle Oxfordian	Spongiolithic limestone
PC-18-48		Non-altered	Bifurcatus Zone, Upper Oxfordian	Spongiolithic limestone
PC-19-06		Non-altered	Bifurcatus Zone, Upper Oxfordian	Spongiolithic limestone
PC-22-04		Non-altered	Bifurcatus Zone, Upper Oxfordian	Spongiolithic limestone
PC-22-41	*Hibolithes*	Non-altered	Bifurcatus Zone, Upper Oxfordian	Spongiolithic limestone
PC-22-NEW	*Hibolithes*	Non-altered	Bifurcatus Zone, Upper Oxfordian	Spongiolithic limestone
PC-25-62		Non-altered	Bifurcatus Zone, Upper Oxfordian	Spongiolithic limestone
PC-31-41	*Hibolithes*	Non-altered	Bifurcatus Zone, Upper Oxfordian	Spongiolithic limestone
PC-31-43	*Hibolithes*	Non-altered	Bifurcatus Zone, Upper Oxfordian	Spongiolithic limestone
PC-31-NEW		Non-altered	Bifurcatus Zone, Upper Oxfordian	Spongiolithic limestone
PC-37-04	*Hibolithes*	Partially altered	Bifurcatus Zone, Upper Oxfordian	Spongiolithic limestone
PC-37-NEW		Partially altered	Bifurcatus Zone, Upper Oxfordian	Spongiolithic limestone
PC-38/39-35	*Hibolithes*	Non-altered	Bimammatum Zone, Upper Oxfordian	Spongiolithic marl-peloidal limestone
PC-39-25	*Hibolithes*	Non-altered	Bimammatum Zone, Upper Oxfordian	Spongiolithic marl-peloidal limestone
PC-39-NEW	*Hibolithes*	Non-altered	Bimammatum Zone, Upper Oxfordian	Spongiolithic marl-peloidal limestone
PC-40/41-43	*Hibolithes*	Non-altered	Bimammatum Zone, Upper Oxfordian	Spongiolithic marl-peloidal limestone
PC-40/41-54	*Hibolithes*	Non-altered	Bimammatum Zone, Upper Oxfordian	Spongiolithic marl-peloidal limestone
PC-41/42-41	*Hibolithes*	Partially altered	Bimammatum Zone, Upper Oxfordian	Spongiolithic marl-peloidal limestone
PC-41/42-42	*Hibolithes*	Non-altered	Bimammatum Zone, Upper Oxfordian	Spongiolithic marl-peloidal limestone
PC-42/43-NEW	*Hibolithes*	Non-altered	Bimammatum Zone, Upper Oxfordian	Spongiolithic marl-peloidal limestone
PC-45-14	*Hibolithes*	Non-altered	Bimammatum Zone, Upper Oxfordian	Spongiolithic marl-peloidal limestone
PC-45-46	*Hibolithes*	Non-altered	Bimammatum Zone, Upper Oxfordian	Spongiolithic marl-peloidal limestone
PC-45-86	*Hibolithes*	Non-altered	Bimammatum Zone, Upper Oxfordian	Spongiolithic marl-peloidal limestone
PC-45-NEW	*Hibolithes*	Non-altered	Bimammatum Zone, Upper Oxfordian	Spongiolithic marl-peloidal limestone
PC-46-12	*Hibolithes*	Non-altered	Bimammatum Zone, Upper Oxfordian	Spongiolithic marl-peloidal limestone
PC-47-19	*Hibolithes*	Non-altered	Planula Zone, Lower Kimmeridgian	Marl-limestone rhythmite
PC-47-04	*Hibolithes*	Non-altered	Planula Zone, Lower Kimmeridgian	Marl-limestone rhythmite
PC-47-NEW	*Hibolithes*	Non-altered	Planula Zone, Lower Kimmeridgian	Marl-limestone rhythmite
PC-48-35	*Hibolithes*	Non-altered	Planula Zone, Lower Kimmeridgian	Marl-limestone rhythmite
PC-49-NEW	*Hibolithes*	Non-altered	Planula Zone, Lower Kimmeridgian	Marl-limestone rhythmite
PC-50-NEW	*Hibolithes*	Non-altered	Planula Zone, Lower Kimmeridgian	Marl-limestone rhythmite
PC-52-37	*Hibolithes*	Non-altered	Planula Zone, Lower Kimmeridgian	Marl-limestone rhythmite
PC-52-58	*Hibolithes*	Non-altered	Platynota Zone, Lower Kimmeridgian	Marl-limestone rhythmite
PC-52-NEW	*Hibolithes*	Non-altered	Platynota Zone, Lower Kimmeridgian	Marl-limestone rhythmite
PC-53-25	*Hibolithes*	Non-altered	Platynota Zone, Lower Kimmeridgian	Marl-limestone rhythmite
PC-57-57	*Hibolithes*	Partially altered	Platynota Zone, Lower Kimmeridgian	Marls
PC-58/59-11	*Hibolithes*	Partially altered	Platynota Zone, Lower Kimmeridgian	Marls
PC-59/60-01	*Hibolithes*	Partially altered	Platynota Zone, Lower Kimmeridgian	Marls